A Wearable Isokinetic Training Robot for Enhanced Bedside Knee Rehabilitation

Yanggang Feng, Xingyu Hu, Yuebing Li, Ke Ma, Jiaxin Ren, Zhihao Zhou, *Member, IEEE*, Fuzhen Yuan, Yan Huang, Liu Wang, Qining Wang, *Senior Member, IEEE*, Wuxiang Zhang, *Member, IEEE*, and Xilun Ding

***Abstract*—Knee pain is prevalent in over 20% of the population, limiting the mobility of those affected. In turn, isokinetic dynamometers and robots have been used to facilitate rehabilitation for those still capable of ambulation. However, there are at most only a few wearable robots capable of delivering isokinetic training for bedridden patients. Here, we developed a wearable robot that provides bedside isokinetic training by utilizing a variable stiffness actuator and dynamic energy regeneration. The efficacy of this device was validated in a study involving six subjects with debilitating knee injuries. During two courses of rehabilitation over a total of three weeks, the average peak torque, average torque, and average work produced by their affected knees increased significantly by 81.0%, 101.4%, and 117.6%, respectively. Furthermore, the device's energy regeneration features were found capable of extending its operating time to 198 days under normal usage, representing a 57.8% increase over the same device without regeneration. These results suggest potential methodologies for delivering isokinetic joint rehabilitation to bedridden patients in areas with limited infrastructure.**

Received 31 October 2024; revised 20 January 2025; accepted 11 March 2025. Date of publication 18 March 2025; date of current version 7 April 2025. This work was supported in part by the National Key Research and Development Program of China under Grant 2022YFB4701200, in part by the National Natural Science Foundation of China under Grant T2121003 and Grant 62073038, in part by the Innovation & Transfer Fund of Peking University Third Hospital under Grant BYSYZHZB110, in part by the Beijing Institute of Technology Research Funds for High-Level Talents, in part by the Fundamental Research Funds for the Central Universities under Grant YWF-23-L-1205, and in part by the "Scientific Innovation Yongjiang 2035" Key Technology Breakthrough Plan Projects in Ningbo City under Grant 2024Z199. This article was recommended for publication by Associate Editor Z. Li and Editor D. Kulic upon evaluation of the reviewers' comments. *(Yanggang Feng and Xingyu Hu contributed equally to this work.) (Corresponding authors: Yanggang Feng; Liu Wang; Qining Wang; Wuxiang Zhang; Xilun Ding.)*

This work involved human subjects or animals in its research. Approval of all ethical and experimental procedures and protocols was granted by the Local Ethics Committee of Beihang University, Application No. BM20240173, and performed in line with the Declaration of Helsinki.

Yanggang Feng, Xingyu Hu, Yuebing Li, Ke Ma, Jiaxin Ren, Wuxiang Zhang, and Xilun Ding are with the School of Mechanical Engineering and Automation, Beihang University, Beijing 100191, China (e-mail: yanggangfeng@buaa.edu.cn; zhangwuxiang@buaa.edu.cn; xlding@buaa.edu.cn).

Zhihao Zhou and Qining Wang are with the College of Engineering, Peking University, Beijing 100871, China (e-mail: qiningwang@pku.edu.cn).

Fuzhen Yuan is with the Department of Sports Medicine, Peking University Third Hospital, Institute of Sports Medicine of Peking University, Beijing 100871, China.

Yan Huang is with the School of Mechatronical Engineering, Beijing Institute of Technology, Beijing 100081, China.

Liu Wang is with the Department of Modern Mechanics, University of Science and Technology of China, Hefei 230027, China (e-mail: wangliu05@ustc.edu.cn).

This article has supplementary downloadable material available at https://doi.org/10.1109/TRO.2025.3552332, provided by the authors.

Digital Object Identifier 10.1109/TRO.2025.3552332

***Index Terms*—Bedside rehabilitation, energy regeneration, isokinetic training, resistance training, variable stiffness joint.**

I. Introduction

THE knee plays a crucial role in facilitating mobility in daily activities, regularly bearing 0.5–7.6 times the body's gravitational resting force at any given time [1]. However, more than 20% of the global population is estimated to suffer from debilitating knee pain [2], [3], [4], corresponding to approximately 1.6 billion people who have previously experienced or are currently living with these conditions [5]. Compounding this issue, an aging global population predicts a higher incidence of chronic degenerative knee pathologies that result in the loss of mobility [6], and this loss of mobility makes it challenging to sustain personal independence in daily life [7], [8].

In recent years, over 18 million people have suffered from acute knee joint injuries [9] that account for 37% of all musculoskeletal injuries [10]. Typically, individuals with congenital disorders or acute knee injuries are advised to rest in bed for several months after surgery [11], [12]. For these bedridden patients, muscle strength may degrade and delay rehabilitation [12], [13], [14]. Consequently, strength training on the bed or at the bedside is recommended [11], [15]. In parallel, isokinetic training [16] has been found to be more effective for enhancing the muscle strength of knee extensors and flexors during the rehabilitation process compared to traditional isometric and isotonic contraction training methods [17], [18]. This is due to the fact that isokinetic training promotes maximum muscle contraction at all knee angles. However, isokinetic training requires an external device, called a dynamometer, to generate the appropriate resistance and maintain a constant joint velocity [19].

Currently, there is an absence of isokinetic training devices tailored for bedridden patients with weak knee muscles [20], [21], [22], [23], [24], [25], [26], [27], [28]. Existing isokinetic dynamometers [20], [21], [22], [23], [24], [25] are primarily designed for patients with relatively strong muscles and healthy athletes (grade 4–5, by manual muscle testing) [29], [30]. They are typically rigid, energy-inefficient, large in size, and heavy [20], [21], [22], [23], [24], [25]. These characteristics make conventional isokinetic dynamometers wholly impractical for bedside training [27], [28]. High medical costs and insufficient hospital resources further impede the general public's access to isokinetic training in any form [28], [31], [32], [33].

TABLE I
PARAMETER COMPARISON

Model	Picture	Use	Clinical stage	Method	Velocity error (120°/s)	Consumed power (W)	Size	Interface	Compliance
PADS [34]		Isometric	Healthy (N=27, 2 trials)	N. A.	N. A.	N. A.	1.3kg, 0.03m^2	Computer screen	None
WDS [35]		Isometric	Healthy (N=35, 2 trials)	N. A.	N. A.	N. A.	2.85kg	Computer screen	None
VRED [36]		Isokinetic	N. A.	Magneto-rheological fluid damper	N. A.	Est. 110	N. A.	None	None
AKROD [38]		Isokinetic	Healthy (N=9, 1 trial)	Electro-rheological fluid damper	Est. >10%	Est. >100	3.18kg	None	None
Ours		**Wearable**	**Patients (N=6, 3 weeks, 12 trials)**	**Regenerative braking**	**4.3%**	**0.45**	**1.3kg, 0.03m^2**	**Smartphone**	**5.0-137.3 Nm/rad**

Fortunately, recent advancements in wearable robotics have provided a scientific understanding of solutions to these limitations that may enable wearable isokinetic robots for bedridden patients. Previous resistance training robots have emphasized portability, for example, portable isometric dynamometers [26], [34], rehabilitation devices with variable resistance [35], [36], and an active knee rehabilitation orthotic device [37]. However, these earlier devices were still uncomfortably rigid and relied on an external power supply due to their relatively high power consumption [35], [37]. In response, compliant isokinetic robots featuring variable stiffness actuators (VSAs) [38], [39], [40], [41], [42] have emerged as a popular design choice. The adoption of VSAs in robotics offers advantages such as safer human–machine interactions (HMIs) [43], lower power consumption [40], [44], and energy-efficient characteristics [45], [46], [47], making them widely applicable in various applications, e.g., rehabilitation robots [48], [49], [50] and compliant prostheses [51], [52], [53].

One quality, in particular, lower power consumption, is essential for untethered wearables intended for bedside and home use. One method to achieve this quality is harvesting negative work for subsequent conversion into electricity in a process known as regeneration [54], [55], [56], [57], [58]. For instance, in the times when an isokinetic robot operates to produce resistive forces, humans are simultaneously performing negative work [20], [21], [22], [23], [24], [25]. Using brushless direct current (BLDC) motors, this negative work can be harvested and converted to electricity for reuse [59], [60], [61]. As a synergistic outcome, improving energy efficiency can also reduce production costs by eliminating extra electrical elements [59], [60], [61], [62], [63].

In this study, we propose a wearable isokinetic robot for bedside knee rehabilitation featuring a highly integrated VSA (VSA, 5.0–137.3 Nm/rad) and an energy regeneration system. Our bedside isokinetic robot bridges the rehabilitation gap between bedridden rest and subsequent ambulatory rehabilitation activities. The robot is capable of achieving the range of stiffness required to maximize the efficacy of isokinetic knee training for patients with weaker knee muscles [see Fig. 1(b)]. It also features remote cloud-based optimization for training parameters [see Fig. 1(a)]. It is portable with a weight of 1.3 kg and power consumption of 0.45 $\pm$ 0.01 W, and it can be produced at a low cost (<$500).

The efficacy of our proposed rehabilitation approach was preliminarily validated through a study involving six subjects with severe knee injuries who used the device over the course of three weeks of bedside training. In doing so, we found that subjects demonstrated significant improvements in metrics related to knee muscle strength and function as a result of our intervention. We further evaluated the device's energy consumption during isokinetic exercise and affirmed that its regenerative circuits enhance the battery endurance of the overall system, making it more suitable for remote deployment.

II. METHODS

The bedside isokinetic training robot consists of three main modules: a back-drivable VSA, a control circuit that includes an isokinetic controller, energy regeneration system, and power system, and a human–robot coupling module, as shown in Fig. 1(a).

A. Design of VSA

The VSA is composed of a variable stiffness gear (Gear 3: 23 teeth, 2 mm module), a spur gear set (Gear 2: 17 teeth; Gear 1: 23 teeth), and a BLDC motor (DJI M3508, reduction ratio 19:1)

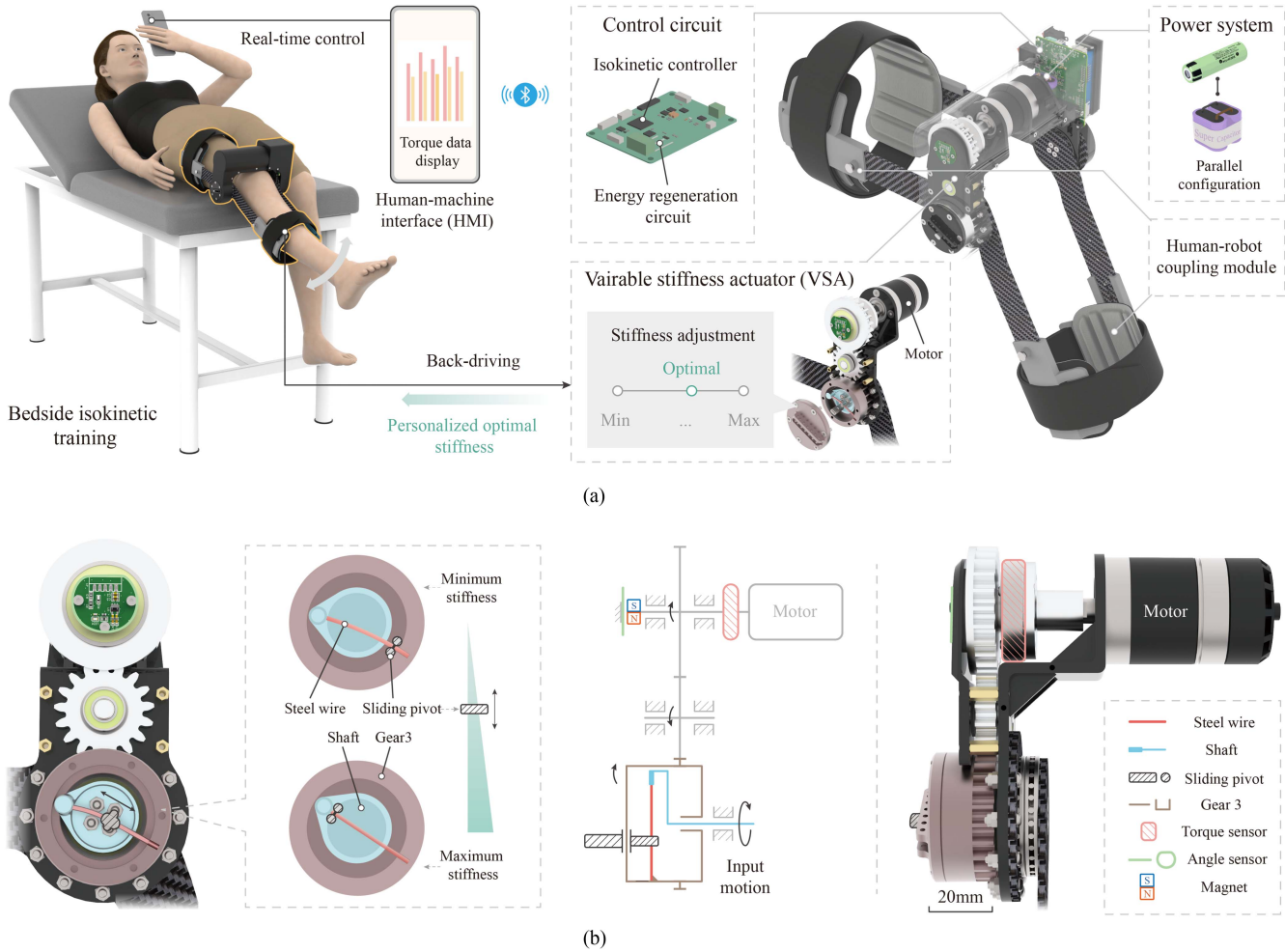

Fig. 1. Variable stiffness isokinetic training robot for bedside rehabilitation of the knee. (a) Bedside isokinetic robot. The robot is donned by the individual who uses a smartphone to control joint velocity and the number of repetitions during isokinetic training. (b) Operating principle of the VSA and mechanism schematics. Stiffness is adjustable by altering the effective length of a compliant steel flexure in series with the motor output.

in series [see Fig. 2(a)]. The full transmission ratio between the rotor of the BLDC motor and the shank rod is 23:17:23 (1:1).

The variable stiffness gear is based on a steel flexure mechanism for a highly integrative and lightweight design. The gear is composed of four custom parts assembled with widely available standardized components. A 304 stainless steel wire [diameter = 2 mm, length = 40 mm, E = 206 GPa, highlighted with red, Fig. 2(a)] serves as the elastic flexure whose two ends are connected to Gear 3 (brown) and the input shaft (blue). The pivot moves linearly along the slide rail of the end cap (fixed to Gear 3 with screws), and the steel flexure passes through the middle of two rollers with a diameter of 3 mm on either side of the point pivot. The position of the pivot determines the effective length (b) of the steel flexure, directly influencing the stiffness between the input shaft and Gear 3 [joint stiffness, denoted as K_j, Fig. 2(b)]. Seven pairs of threaded holes corresponding to seven different stiffnesses on the slide rail are made available upon locking the pivot [see Fig. 2(b)].

Stiffness, i.e., the ratio of torque (M) to angular displacement (θ_j) [Fig. 2(c), $n = 9$], is measured by the torque sensor (LZ-NJY40, 0-15 Nm, Lizhi, Hefei, China) and a magnetic encoder installed concentrically upon the joint. A torque wrench is used to calibrate the torque sensor. The entire variable stiffness gear assembly weighs 0.12 kg and produces a wide range of stiffness [5.0–137.3 Nm/rad, gray 5.0 ± 0.5, yellow 5.3 ± 0.3, green 6.2 ± 0.2, red 7.7 ± 0.2, orange 12.8 ± 0.2, purple 38.4 ± 2.2, blue 137.3 ± 16.6 (mean $\pm$ 95% s.e.m.)]. To measure stiffness, small-scale rotations ($0.5 - 6°$) were applied to the input shaft while maintaining Gear 3 in a fixed position. The theoretical stiffness of the mechanism (K_{the}) can be estimated by the following:

$$K_{\text{the}} = \frac{3EIa^2\epsilon}{b^3} = \frac{3Ed^4a^2\tau(\theta_j)}{(29-l)^3} \quad (1)$$

where $b = 29$ - l mm, $E = 206$ GPa, $I = \pi d^4/64$, $d = 2$ mm, and $a = 11.5$ mm according to the design parameters. τ is a function of θ_j [42].

The VSA weighs 0.74 kg and is integrated on the right side of the robot (from the user's perspective). The maximum shear force applied to the stainless steel flexure is 1306.2 N (equivalent shear strength = 416 Mpa). Therefore, the maximum load of the VSA is 15.0 Nm. Gear 1, Gear 2, the flange, Gear 3 (output),

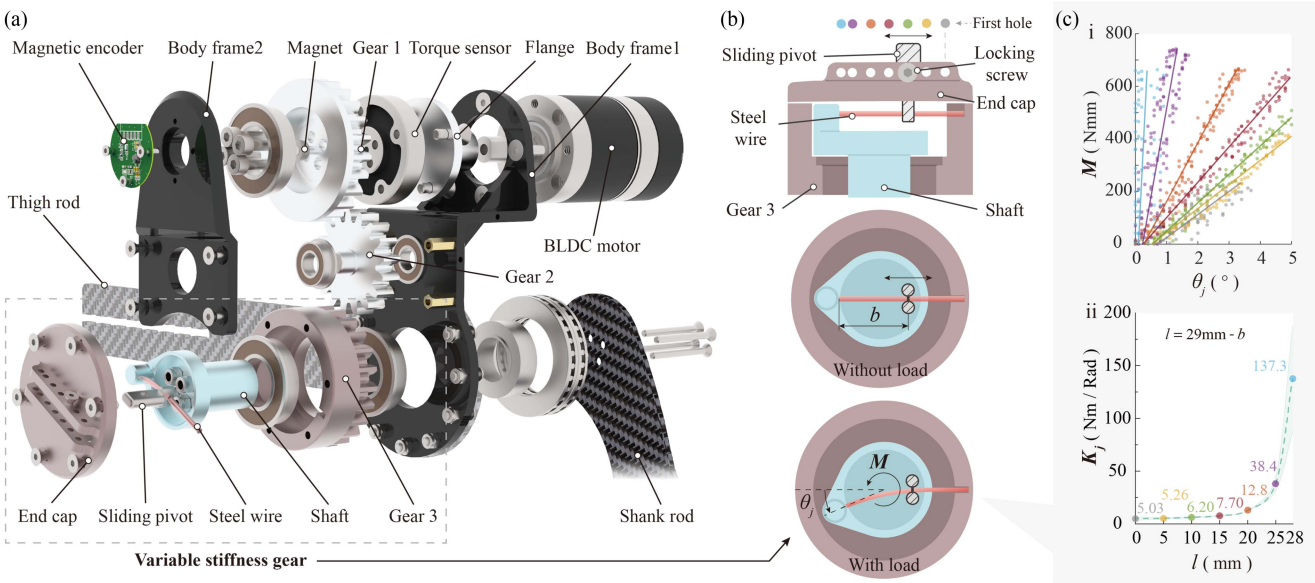

Fig. 2. Mechanical characteristics of the backdrivable VSA. (a) Exploded view of the VSA. Assuming the thigh rod is fixed, extension and flexion of the knee are transmitted through the shank to the shank rod. This movement drives variable stiffness gear and ultimately back-drives the motor with a reduction ratio of 1:1. (b) Variable stiffness gear based on variable length flexure. Seven pairs of threaded holes are arranged linearly to enable the selection of seven different stiffnesses. The centerline distance between the sliding pivot and the steel flexure's end is denoted as b, and l =29 mm-b is the centerline distance between the sliding pivot and the first hole on the right (gray point). The steel flexure's end is connected to the driveshaft. (c) Stiffness characteristics of the VSA. Different colors represent different threaded hole selections in Fig. 2(b). (i) Torque vs. angular displacement ($M - \theta_j$) at different stiffnesses. (ii) Stiffness versus centerline distance ($K_j - l$) curve.

the shaft (input), and the end cap (black anodized) are made of 6061 aluminum alloy by computer numerical control (CNC) machining. To mitigate abrasion between the pivot and the steel flexure, the pivot is made of carbon steel 45. By utilizing the available volume provided by Gear 3's hollow design, the variable stiffness mechanism is able to achieve a diameter of 50 mm and a height of 55 mm.

The variable stiffness gear weighs 0.12 kg with a corresponding size of 50×50×55 mm. It combines a transmission gear with a variable stiffness mechanism. Its low weight and compact size contribute to the wearability and portability of the robot.

B. Human–Robot Coupling Module

The design of the human–robot coupling module was driven by anatomical design heuristics [64], [65]. Considering the coordination required between the thigh and shank cuffs, the circuit board and power system are mounted on two robot body frames to accommodate lower limbs of different sizes (Supplementary Fig. 11). The frame is 3D-printed using polylactic acid (PLA). The thigh rod and shank rod are made of carbon fiber reinforced plastic (CFRP) plates with a thickness of 3 mm. The hole arrays on the thigh and shank rods are used to adjust the cuffs' positions to fit individuals with differing limb measurements. The straps and cuffs come from a knee orthosis (Medwe, Jiapu, Tianjin, China). The casings of the bedside isokinetic robot are formed by stereo lithography appearance (SLA) 3-D printing with a thickness of 2 mm.

C. Controller and Sampling

A 32-bit microcontroller unit (MCU, STM32F405, STMicroelectronics) is utilized for control and sampling (Supplementary Fig. 12). The signals containing information about angle, torque, and supercapacitor voltage are all sampled at a rate of 100 Hz. The actual velocity of the knee is calculated from calibrated angular measurements. A proportional–integral (PI) controller processes the error between the actual and desired velocities, and the control parameters (PWM duty cycles) are transmitted to the driver circuit in real time. Three-channel PWMs are received by a motor driver (DRV8323S, Texas Instruments) that communicates with the MCU through the serial peripheral interface (SPI) communication protocol. Magnetic encoders (TLE5012B, Infineon, resolution 0.01°) are employed for angular measurement and communicate with the MCU through the SPI protocol. The sensitivity of a torque sensor is 1.0 ± 0.01 mV/V. An operational amplifier (AD8221, Analog Devices) amplifies the torque sensor's differential signal by 991 times for subsequent measurement by the analog-to-digital conversion (ADC) channel of the MCU. The voltage of the supercapacitor is also measured by an ADC channel of the MCU.

D. Power System

A lithium battery (Panasonic NCR18650, 3.7 V) with a capacity of 3800 mAh powers the device. The battery is wired in parallel with a supercapacitor with a capacity of 10 F and a voltage of 5.5 V. A diode is used to prevent charging current from back-flowing from the battery to the supercapacitor. To achieve a stable power supply, a boost circuit is employed to convert the voltage from the battery-capacitor system to a voltage of 12 V. In consideration of the working voltage of each component, a step-down chip (TPS54360DAR, Texas Instruments) is used to obtain a voltage of 5 V to power the magnetic encoder and

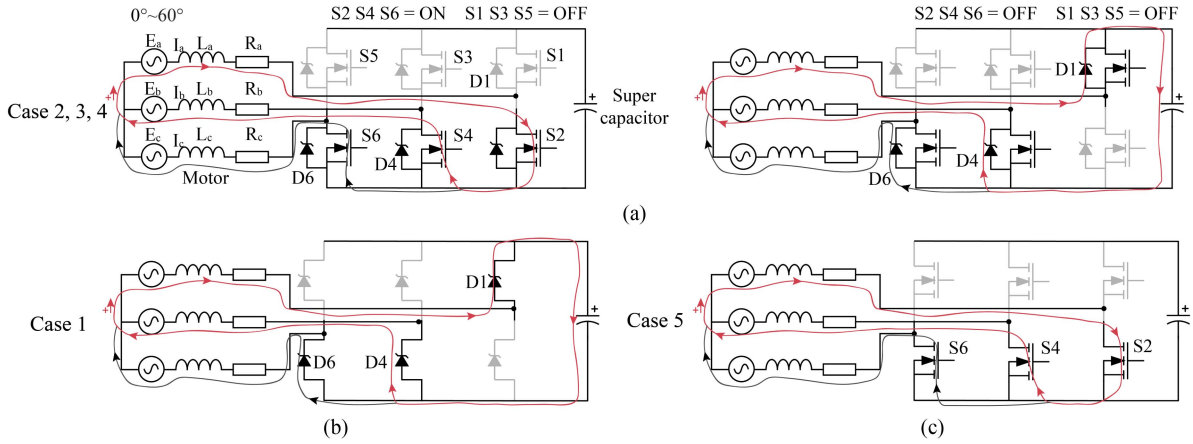

Fig. 3. Equivalent energy regeneration circuit. (a) Cases 2, 3, 4. The MOSFETS S2, S4, and S6 are ON/OFF. (b) Case 1. MOSFETS S2, S4, and S6 are always OFF during the whole cycle and diodes direct the flow of the charging current when $(E_a - E_b)_{\max} > U_c + 2U_d$. (c) Case 5. MOSFETS S2, S4, and S6 are ON during the entire cycle.

the torque sensor. In addition, a low dropout voltage regulator (AMS1117-3.3, Advanced Monolithic Systems) generates a voltage of 3.3 V based on the reference voltage of 5 V to power the MCU.

E. Dynamic Energy Regeneration

Dynamic energy regeneration in the BLDC motor is achieved based on the boost principle. By controlling the ON/OFFstates of the MOSFETS around the motor, the current can be redirected to the supercapacitor-battery subsystem of the wearable robot. When low-side MOSFETS are ON, the motor windings are shortened. When low-side MOSFETS are suddenly switched OFF, the energy stored in the inductance of the circuit cannot disappear suddenly, and the motor windings produce an induced electromotive force (EMF). The induced EMF is the voltage that charges the supercapacitor (see Fig. 3). This dynamic energy regeneration method eliminates the need for additional circuits beyond those required for motor control, enabling energy regeneration to be directly implemented with the existing circuit topology.

The braking and energy regeneration circuit consisting of three individual phases a, b, and c is composed of the equivalent resistors R_a, R_b, and R_c, the equivalent inductances L_a, l_h, and L_c, and the back EMFs E_a, E_b, and E_c. As shown in Fig. 3, PWM regulates the ON/OFF status of MOSFETS $S2$, $S4$, and $S6$ while $S1$, $S3$, and $S5$ are kept OFF in all operating regimes. The phase currents of the three phases are represented by I_a, I_b, and I_c.

When MOSFETS $S2$, $S4$, and $S6$ are switched ON, the back EMFs and currents on phases a and b are expressed as $E_{a_{\text{on}}}$, $E_{b_{\text{on}}}$, $I_{a_{\text{on}}}$, and $I_{b_{\text{on}}}$, respectively. According to Kirchhoff's Voltage Law, the corresponding differential equation while MOSFETS $S2$, $S4$, and $S6$ are ON, as shown in Fig. 3(a), can be expressed as

$$E_{b_{\text{on}}} - E_{a_{\text{on}}} = (R_a + R_s)I_{a_{\text{on}}} + (R_b + R_s)I_{b_{\text{on}}} + L_a\frac{dI_{a_{\text{on}}}}{dt_{a_{\text{on}}}} + l_h\frac{dI_{b_{\text{on}}}}{dt_{a_{\text{on}}}} \tag{2}$$

where R_s represents the equivalent resistance of MOSFETS $S2$ and $S4$, and $t_{a_{\text{on}}}$ indicates the rise time of the current $I_{a_{\text{on}}}$.

When MOSFETS $S2$, $S4$, and $S6$ are switched OFF, the back EMFs and currents on a and b are expressed as $E_{a_{\text{off}}}$, $E_{b_{\text{off}}}$, $I_{a_{\text{off}}}$, and $I_{b_{\text{off}}}$, respectively. According to Kirchhoff's Voltage Law, the corresponding differential equation while MOSFETS $S2$, $S4$, and $S6$ are OFF can be expressed as

$$E_{b_{\text{off}}} - E_{a_{\text{off}}} = R_aI_{a_{\text{off}}} + R_bI_{b_{\text{off}}} + U_c + 2U_d + L_a\frac{dI_{a_{\text{off}}}}{dt_{a_{\text{off}}}} + l_h\frac{dI_{b_{\text{off}}}}{dt_{a_{\text{off}}}} \tag{3}$$

$$I_{a_{\text{off}}} = C\frac{dU_c}{dt} \tag{4}$$

where U_d refers to the diode forward conduction voltage of $D1$ and $D4$, and U_c and C represent the voltage and capacitance of the supercapacitor, respectively. $t_{a_{\text{off}}}$ indicates the falling time of the current $I_{a_{\text{off}}}$.

The increase in current $dI_{a_{\text{on}}}$ through inductor L_a can be estimated as equal to the decrease in current $dI_{a_{\text{off}}}$. Thus, the average current $\overline{I_a}$ flowing through the equivalent inductor L_a in one cycle can be expressed as

$$\overline{I_a} = \frac{E_b - E_a - (1-D)(\overline{U_c} + 2U_d)}{2(R_a + R_sD)} \tag{5}$$

where $\overline{U_c}$ refers to the average voltage of the supercapacitor. D is the duty cycle of the PWM that regulates the ON/OFF state of MOSFETS $S2$, $S4$, and $S6$. The supercapacitor only recovers energy when the average current $\overline{I_a} \geq 0$. The expression that determines when the supercapacitor charges is

$$D \geq D_0 = 1 - \frac{E_b - E_a}{\overline{U_c} + 2U_d} \tag{6}$$

where D_0 is the minimum PWM duty cycle that will charge the supercapacitor.

The overall behavior of the regeneration circuit can be described by several states. In case 1, all MOSFETS are switched OFF because $D = 0$. The circuit is simplified to six diodes in

operation and the equivalent circuit is shown in Fig. 3(b). For cases 2, 3, and 4, it is roughly estimated that the circuit current does not change abruptly in one cycle, thus $\overline{I_a}$ is equal to $\overline{I_{\text{reg}}}$, when MOSFETS S2, S4, and S6 are OFF, as shown in Fig. 3(a). However, in case 5 as shown in Fig. 3(c), the current does not flow into the supercapacitor.

1) *Case 1.1*: $D = 0$ & $(E_a - E_b)_{\max} \le U_c + 2U_d$.
2) *Case 1.2*: $D = 0$ & $(E_a - E_b)_{\max} > U_c + 2U_d$.
3) *Case 2*: $0 < D < 1$ & $D_0 \le 0$ & S2, S4, S6 = OFF.
4) *Case 3*: $0 < D < D_0$ & $D_0 > 0$ & S2, S4, S6 = OFF.
5) *Case 4*: $D_0 < D < 1$ & $D_0 > 0$ & S2, S4, S6 = OFF.
6) *Case 5*: $D = 1$ or S2, S4, S6 = ON.

The charging current I_{reg} can be expressed as follows:

$$I_{\text{reg}} = \begin{cases} 0 & Case\,1.1 \\ \frac{(E_b - E_a)e^{-t/(R_a+R_b)C}}{R_a+R_b} & Case\,1.2 \\ \frac{E_b - E_a - ((1-D)(\overline{U_c}+2U_d))}{2(R_a+R_sD)} & Case\,2 \\ \left(0, \frac{E_b - E_a - ((1-D)(\overline{U_c}+2U_d))}{2(R_a+R_sD)}\right) & Case\,3 \\ \frac{E_b - E_a - ((1-D)(\overline{U_c}+2U_d))}{2(R_a+R_sD)} & Case\,4 \\ 0 & Case\,5 \end{cases} \tag{7}$$

$$E_b - E_a = k_g \omega_r \tag{8}$$

where k_g is the generator constant of the motor (V/rpm), and ω_r is the angular velocity of the rotor. The regeneration power P_{reg} can be calculated by

$$\begin{aligned} P_{\text{reg}} &= \frac{\Delta Q_c}{\Delta t} = \frac{C(U_{c2}^2 - U_{c1}^2)}{2(t_2 - t_1)} \\ &= \frac{(\int_0^{t_2} I_{\text{reg}} dt)^2 - (\int_0^{t_1} I_{\text{reg}} dt)^2}{2C(t_2 - t_1)} \end{aligned} \tag{9}$$

where U_{c1} and U_{c2} indicate the voltage of the supercapacitor at start time t_1 and end time t_2 of the energy regeneration, respectively. ΔQ_c represents the energy harvested by the supercapacitor.

F. Closed-Loop Isokinetic Control

Isokinetic training is characterized by enforcing a constant joint velocity during maximal volitional limb movements (see Fig. 4). When the actual knee velocity is greater than the desired velocity, the duty cycle of the PWM (D) increases, and consequently, the motor generates more resistance against the shank. The opposite is true when the actual knee velocity is lower than the desired velocity. In that case, D decreases to lower resistance against the shank. As indicated by the green arrow in Fig. 4, kinetic energy from knee extension and flexion is transformed into the stored elastic energy of the variable stiffness gear. Subsequently, the stored elastic energy of the steel flexure rotates the gear set, which, in turn, rotates the motor shaft (back-drives the motor). The motor works as a generator, transforming mechanical energy into electrical energy by inducing current through six MOSFETS. These in turn charge the supercapacitor in parallel with the battery to power the system.

The feasibility of generating resistance through dynamic energy regeneration was verified at different target velocities and

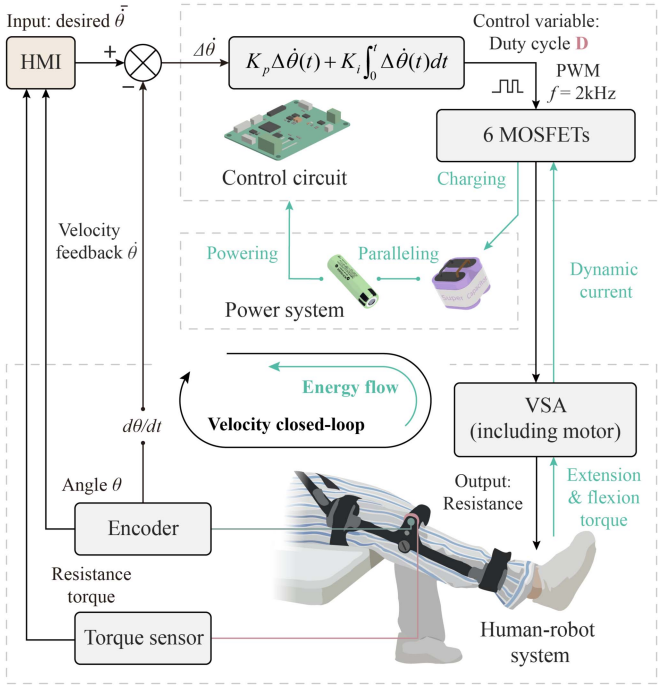

Fig. 4. Closed-loop isokinetic control along with energy regeneration. Knee angle θ is measured by a magnetic encoder at a sampling rate of 100 Hz. Torque data is displayed on the HMI panel in real-time after processing. Closed-loop isokinetic control is achieved by a PI controller, which processes the error ($\Delta\dot{\theta}$) between actual velocity $\dot{\theta}$ and desired velocity $\bar{\dot{\theta}}$. K_p and K_i are proportional gain and integral gain, respectively. The controller switches low-side MOSFETS ON and OFFby PWM. The duty cycle D determines the braking resistance from the motor and variable stiffness gear applied to the lower limb. The motor simultaneously acts as a generator, and the supercapacitor (10 F, 5.5 V) harvests the electrical energy to power the system in conjunction with the battery in parallel.

loads (see Fig. 5). To evaluate isokinetic performance at different loads, an individual subject (Subject 6) performed active knee extension and flexion movements five times while targeting average peak torques around 1, 3, and 5 Nm with the desired velocity set to 120°/s. To evaluate the robot's isokinetic performance at different velocities (60°/s, 120°/s, and 180°/s), the subject performed active knee extension and flexion movements 5 times while ensuring that the average peak torque was around 2 Nm (medium load). As shown in Fig. 5, the wearable robot performs best (velocity error 1.2%) under a load of 3 Nm. At a velocity of 120°/s and under different loads, the average velocity error is still only 4.3% .

G. Human–Robot Biomechanical Model in Isokinetic Training

The knee joint can be considered as a biomechanical system comprising two skeleton bones, the femur and tibia, and two antagonistic muscle groups, the quadriceps femoris (dominating knee extension) and hamstrings, as shown in Fig. 6. The angle between the femur and tibia denotes the knee angle θ, and $\dot{\theta}$ represents the angular velocity of knee flexion and extension. F_q is the contractile force of the quadriceps femoris, F_h is the force of the hamstrings, and G is the force of gravity on the shank. The moment arm of the three forces are l_q, l_h, and l_G,

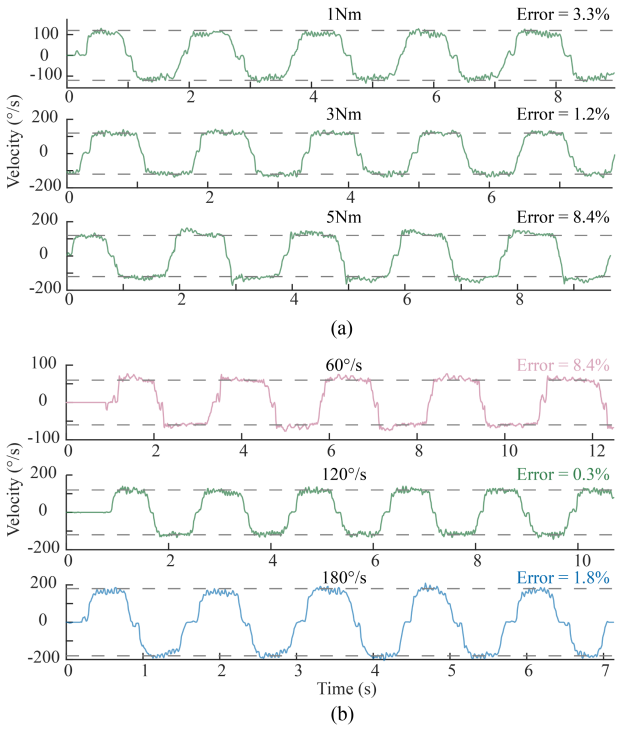

Fig. 5. Isokinetic tracking performance at various loads and velocities. Dashed lines and solid lines represent the desired knee velocities and actual velocities, respectively. (a) Velocity trajectories with average peak torques of 1, 3, and 5 Nm, 120°/s. (b) Velocity trajectories at different desired velocity settings, 2 Nm.

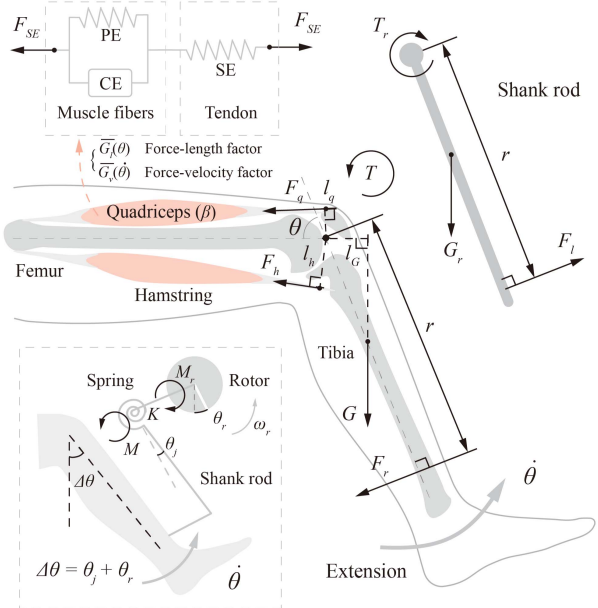

Fig. 6. Biomechanical model of knee extension in isokinetic training.

respectively. T is the overall torque from the knee, which is exerted on the isokinetic training robot.

In equilibrium, the torque T is equal to the sum of the contractile torques of the quadriceps femoris (T_q), hamstrings (T_h), and torques generated by the weight of shank (T_G)

$$T = T_h + T_q + T_G. \tag{10}$$

The torques may be expressed as $T_h = F_h l_h$, $T_q = F_q l_q$, and $T_G = G l_G$.

Muscles can be regarded as a combination of a serial element (SE), contractile element (CE), and parallel element (PE) according to the three-element Hill muscle model [66], as shown in Fig. 6. In particular, the total contractile force of the quadriceps femoris is equal to the force of the SE (F_{SE}), which is the summation of the contractile force of the CE (F_{CE}) and the passive force of the PE (F_{PE}), i.e., $F = F_{\text{CE}} + F_{\text{PE}}$. F_{CE} can be described as a function involving four factors [67], i.e., the maximum voluntary contractile force (MVC, denoted by F_m), the activation level (α), the force–length factor (g_l), and the force–velocity factor (g_v). F_{PE} can be considered negligible over most of the range of motion with a peak of less than 10% of F_m at the maximum anatomical length [68], i.e., $F_{\text{PE}} = 0$. Thus, in this study, F_q is equal to

$$F_q \approx F_{\text{CE}} = \alpha F_m g_l g_v. \tag{11}$$

Due to the low co-activity level supported by literature [69], [70], [71], the hamstrings are assumed to not contribute to co-contraction during maximum knee extension efforts, i.e., $T_h = 0$. After performing gravitational taring, i.e., $T_G = 0$, the torque T is composed of T_q exclusively

$$T \approx T_q = F_q l_q \approx F_{\text{CE}} l_q. \tag{12}$$

During knee extension, T_p is denoted as the peak torque or maximum extension torque generated by the quadriceps femoris. In the knee musculoskeletal system, extension torque also depends on the muscle activation level α, the knee angle θ, and angular velocity $\dot{\theta}$ [67]

$$T \approx \alpha T_p \overline{g_l}(\theta) g_v(\dot{\theta}) \tag{13}$$

$$\overline{g_l}(\theta) = \frac{F_m l_q(\theta) g_l(\theta)}{T_p}. \tag{14}$$

The muscle activation level α can be described as a function of the circumferential strain s for isometric flexions [72], [73], [74]. An approximation of activation level is assumed as follows, where $b = 0$, k_1, and k_2 are functions of knee angle and angular velocity, respectively [72]:

$$\alpha = \alpha(s) \approx ks + b \tag{15}$$

$$k = k_1(\theta) k_2(\dot{\theta}). \tag{16}$$

Substituting (15) and (16) into (13)

$$T \approx s T_p G_l(\theta) G_v(\dot{\theta}) \tag{17}$$

$$G_l = k_1(\theta) \overline{g_l}(\theta) \tag{18}$$

$$G_v = k_2(\dot{\theta}) g_v(\dot{\theta}). \tag{19}$$

Thus, $s_{\max}(\theta)$ is the maximum circumferential strain obtained in isometric MVC flexions at knee angle θ, and β ($0 \le \beta \le 1$) is the normalized circumferential strain, which is the ratio of s to $s_{\max}(\theta)$ [72]. The final knee joint torque model is

$$T \approx \beta T_p \overline{G_l}(\theta) \overline{G_v}(\dot{\theta}) \tag{20}$$

$$\overline{G_l} = \frac{k_1(\theta) s_{\max}(\theta) F_m l_q(\theta) g_l(\theta)}{T_p} \tag{21}$$

IEEE Transactions on Robotics (T-RO) paper, presented at ICRA 2026, Vienna, Austria. Cite as T-RO paper.

$$\overline{G_v} = k_2(\dot{\theta})g_v(\dot{\theta}). \tag{22}$$

Upon extension, the torque of the knee extensors should be equal to the sum of the total resistance torque provided by the robot and the gravity compensation torque. As shown in Fig. 6, the equilibrium equation of the shank rod when the knee extends can be expressed as

$$T_{F_l} - T_{G_r} - T_r = I_r\alpha_r \tag{23}$$

where T_{Fl} and T_{G_r} refer to the moment of the segment force F_l around the axis of rotation of the robot and the shank rod gravity G_r in the robot, respectively. T_r and I_r represent the resistance torque generated by the robot and the moment of inertia of the shank rod, respectively. α_r indicates the angular acceleration of the shank rod. For the lower leg, The equilibrium equation can be expressed as

$$T - T_{F_r} - T_G = I_j\alpha_j \tag{24}$$

where T refers to the aforementioned overall torque exerted on the isokinetic robot by the knee, and T_{F_r} represents the moment of the robot resistance force F_r around the axis of rotation of the joint. I_j and α_j indicate the moment of inertia of the lower leg and the angular acceleration of the lower leg, respectively. α_r and α_j are assumed equal to zero during isokinetic movements, thus the following equation can be obtained to calculate the net muscle torque based on the data from the torque sensor

$$T = T_r + T_{G_r} + T_G \tag{25}$$

When the knee flexes, the knee flexion torque should be equal to the resistance torque less the gravity compensation torque. The equilibrium equation when the knee flexes is

$$T_{F_l} + T_{G_r} - T_r = I_r\alpha_r \tag{26}$$

$$T - T_{F_r} + T_G = I_j\alpha_j \tag{27}$$

$$T = T_r - T_{G_r} - T_G. \tag{28}$$

For active knee extension during isokinetic training, the knee angle and velocity characteristics can be analyzed to establish connections with the energy regeneration models mentioned above. For convenience, the sum of T_{G_r} and T_G is denoted as total gravity compensation T_c, i.e., $T_c = T_{G_r} + T_G$. The variable stiffness mechanism can be regarded as a spring with adjustable stiffness coefficient K (the elastic moment is denoted as M), and the BLDC motor can be regarded as a damper (the resistance moment is denoted as M_r). Thus, the proposed robot can be simplified as a human-spring-damping series system

$$T - T_c = M = K\theta_j. \tag{29}$$

When $T - T_c < M_{r_0}$ (the minimum resistance moment of the motor), the steel flexure in the variable stiffness mechanism deforms (θ_j) simultaneously with the increase in M, and knee angular displacement $\Delta\theta$ is equal to θ_j. When $T - T_c \geq M_{r_0}$, the rotor is back-driven (displacement θ_r) and M_r increases through generation damping, resulting in $\Delta\theta = \theta_j + \theta_r$ as shown in Fig. 6. When $T - T_c = M_r$, the limb maintains isokinetic movement, and the torque equilibrium equation and angle equation are

$$T - T_c = M = M_r = K_t I_a \tag{30}$$

where K_t is the motor torque constant

$$\Delta\theta = \theta_j + \theta_r = \frac{T - T_c}{K} + \theta_r \tag{31}$$

$$\dot{\theta} = \dot{\theta_j} + \dot{\theta_r} = \frac{(T(t) - T_c(t))'}{K} + \omega_r. \tag{32}$$

For isokinetic training, $\dot{\theta}$ is a programmed constant $\dot{\theta_0}$ (60, 120, 180°/s ideally). Substituting (32) into (8) yields

$$E_b - E_a = k_g\left(\dot{\theta_0} - \frac{(T(t) - T_c(t))'}{K}\right). \tag{33}$$

Before the knee extension movement is completed, knee angular velocity, $T - T_c$, and θ_j decrease ($T - T_c < M_r$), and $\Delta\theta = \theta_j + \theta_r$. When the knee velocity reaches zero, the rotor continues to rotate with the release of elasticity and will stop under the condition of $K\theta_j = M_{r_0}$. During knee flexion, the device's moment equilibrium equation and velocity can be obtained by replacing $T - T_c$ in the above equation with $T + T_c$.

Thus, the relationship between muscle contraction, variable stiffness, and energy regeneration is established according to (20), (33), (7), and (9).

H. Human–Machine Interface

A smartphone serves as the HMI to control the bedside isokinetic robot and display torque data. For validation, an Android application named "Isokinetic Training Assistant" was developed and installed on an Android smartphone (Redmi K60, Xiaomi Inc.) with a 6.67-in. touchable screen. The application integrates five functions: (1) user account management; (2) parameters control; (3) data analysis and display; (4) real-time cloud upload; and (5) local historical data display. Upon entering the application interface for the first time, individuals are required to register an account for personal training data storage. After logging in and establishing a Bluetooth connection with the bedside isokinetic robot, users can set up isokinetic training parameters for knee extension-flexion, e.g., velocity, repetition number, and training mode (dynamic/plugging mode, open loop mode). By touching the "Start" button, data from the bedside isokinetic robot begins streaming and training begins. Peak torque and average torque for extension and flexion are calculated and displayed on the panel. Raw data of torque and angle are subsequently uploaded to the cloud server through WiFi, enabling remote diagnosis and treatment by professional physiotherapists or rehabilitation experts. Simultaneously, historical data is stored locally for convenient viewing at any time.

I. Data Collection and Analysis

All data were collected by PC software programmed in Java (version 17). The software features a graphical user interface (GUI) to communicate with the isokinetic robot either over WiFi (2.4 GHz) or universal synchronous/asynchronous receiver/transmitter (USART). An oscilloscope panel is placed in the software interface for real-time observation of sensor signals.

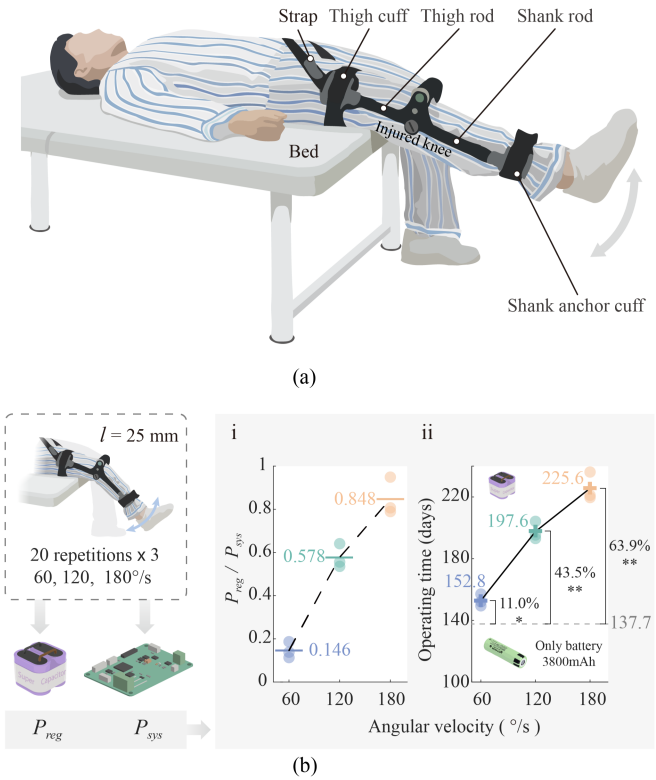

Fig. 7. Experimental setup and operating time improvement with dynamic energy regeneration. (a) Experimental setup. The subject lies in bed. A rod is attached to the shank using a bridle mount system while a separate rod is secured to the thigh. A strap is employed to prevent the robot from slipping off distally. (b) Operating time improvement using energy regeneration. The energy regeneration experiment was conducted before the three weeks of training performed by all subjects. The charging power of the supercapacitor and the total system power are denoted as P_{reg} and P_{sys}, respectively. (i) P_{reg} /P_{sys} at 60, 120, 180°/s, representing the proportion of regenerative energy that can cover the overall system's demands. (ii) Improvement in battery life at three tested velocities (Panasonic NCR18650 lithium battery, 3.7 V, 3.8Ah). Horizontal lines denote group means. ∗P<0.1; ∗∗P<0.01 (paired-sample *T*-test).

The sensor signals that change over time were packaged as files with the extension. mcvs and decoded and analyzed by MATLAB (version R2017b). All statistical tests were conducted using SPSS Statistics 26 software.

III. Subject Experiments

A. Energy Efficiency Improvement

A single patient (male, 26 years old, Subject 1) with a knee articular cartilage injury [75] was recruited to participate in an energy regeneration experiment. The subject provided written and informed consent, having read and understood the potential risks involved. Experimental procedures on the individuals were conducted by protocols approved by the Local Ethics Committee of Beihang University, China (no. BM20240173). As shown in Fig. 7(a), the participant was positioned on a medical bed with the bedside isokinetic robot affixed to his injured knee. The thigh rod and shank rod were secured using a thigh cuff and shank anchor cuff to ensure a tailored fit to the leg's conical shape. To prevent the bedside isokinetic robot from slipping distally, a strap was looped around the hip and appropriately tensioned. Before initiating the extension-flexion isokinetic training, the coaxial alignment between the joint axis of the robot and the participant's knee axis was carefully adjusted to ensure safety and unimpeded movement.

The experiment was conducted to assess the robot's energy regeneration efficiency at 60, 120, and 180°/s [see Fig. 7(b)] before any further rehabilitation training (see Fig. 8). The participant was asked to complete 20 repetitions of extension and flexion with maximum force and maximum range of motion at each of the 3 desired isokinetic velocities. For these trials, the stiffness of the variable stiffness gear was adjusted to the optimal value for the subject according to the methods of Section III-B (see Fig. 9(a), $l = 25$ mm, 38.4 Nm/rad).

When drawing power from only the Panasonic NCR18650 lithium battery (3.7 V, 3.8 Ah), the estimated operating time of the bedside isokinetic robot can be derived from the system's consumed power, denoted as P_{sys}. P_{sys} was measured as 0.45 ± 0.01 W by a regulated power supply. At the sustained working current (I_{sys}, 0.053 A) of the robot, the battery can theoretically power the robot for nearly 52 h. (t_b) according to (34). Assuming that isokinetic training is conducted every other day with each training session lasting 45 min (H) and that the discharge efficiency of the supercapacitor is 95%, the improved battery duration t_{bc} (converted to days) brought by energy regeneration can be estimated by

$$t_b = \frac{C_b \eta}{I_{\text{sys}}} \tag{34}$$

$$t_{\text{bc}} = \frac{2\eta(C_b U_b + \sigma P_{\text{reg}} t_{\text{reg}})}{I_{\text{sys}} U_b H} \tag{35}$$

where η is the battery discharge efficiency (0.72), and σ is the discharge efficiency of the supercapacitor (0.95).

When considering the contributions of energy regeneration, $P_{\text{reg}}/P_{\text{sys}}$ (9) increases with increasing angular velocity and represents the proportion of regenerative energy that can meet the overall system's demands [see Fig. 7(b)i, $14.6 \pm 2.2\%$ at 60°/s, $57.8 \pm 3.2\%$ at 120°/s, $84.8 \pm 5.1\%$ at 180°/s]. Utilizing regenerated energy results in a operating time improvement of $11.0 \pm 1.6\%$ at 60°/s, $43.5 \pm 2.4\%$ at 120°/s, $63.9 \pm 3.8\%$ at 180°/s when compared to baseline operating time without energy regeneration [see Fig. 7(b)ii]. With energy regeneration, the corresponding total working duration can be extended to 153 days at 60°/s, 198 days at 120°/s, and 226 days at 180°/s, respectively.

B. Optimal Stiffness Selection and Effect Validation

To demonstrate the efficacy of the robot, six patients with knee injuries were recruited to undergo bedside isokinetic training. Detailed subject information is shown in Table II. Among the six subjects, there was one case of articular cartilage injury (ACI, right, Subject 1), one case of anterior cruciate ligament rupture (ACL, left, Subject 2), one case of meniscus injury (MI, right, Subject 3), one case of patellar injury (PI, left, Subject 4), and two cases of anterior cruciate ligament rupture with meniscus tear (ACLM, left, Subjects 5 and 6).

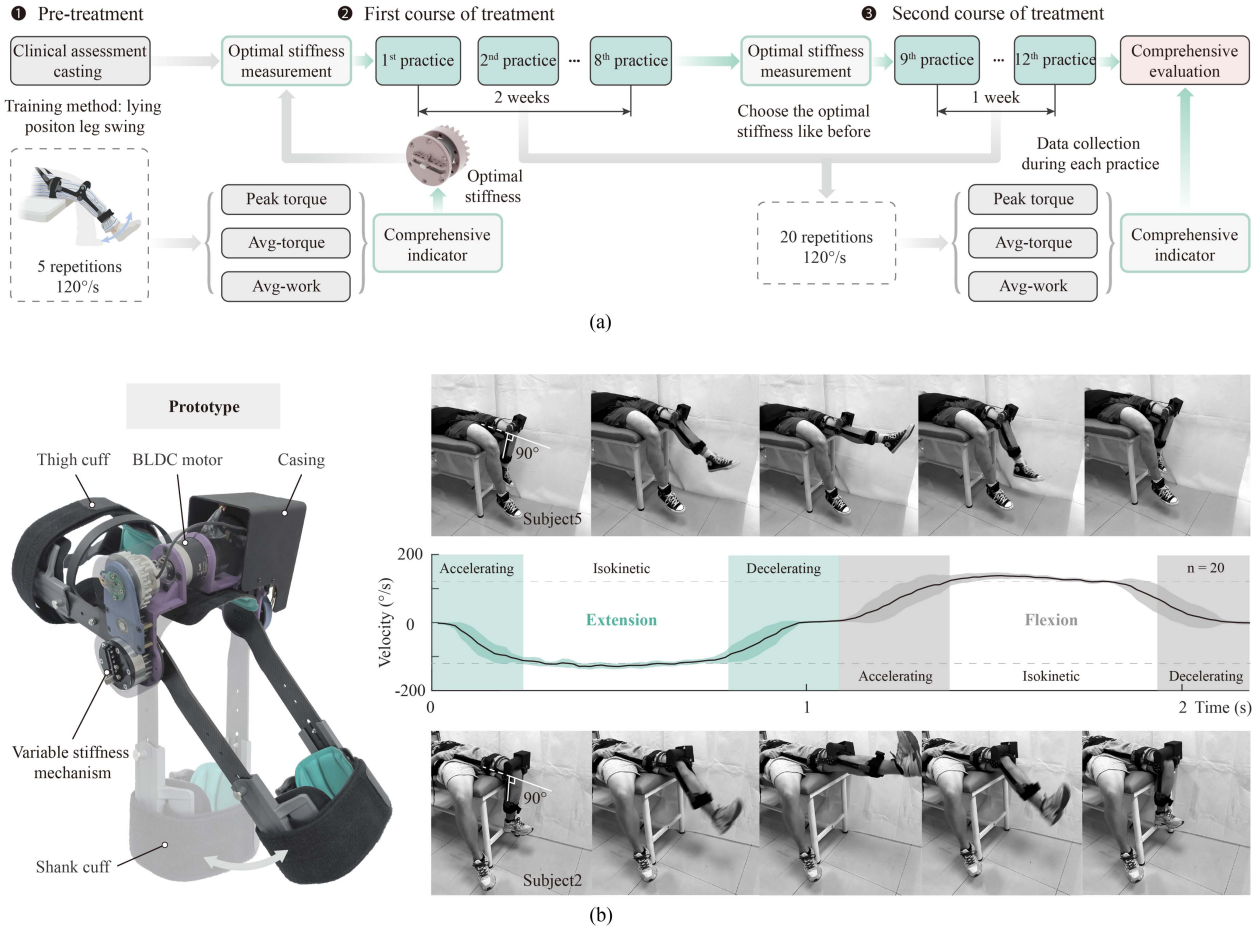

Fig. 8. Rehabilitation trial period. (a) Visit occurrences during 3-week training. In the first course of treatment (Course 1, 2 weeks), the optimal robot stiffness matching the subject's knee was determined according to a CI ((37)) based on peak torque (PT), average torque (AT), and average work (AW) in one extension-flexion cycle. Subsequently, 8 practice sessions over 2 weeks were conducted. Course 2 (1 week) involved 4 practice sessions during which the pre-practice optimal stiffness was measured. (b) Demonstration of the robot during an isokinetic knee training cycle (an extension-flexion repetition).

TABLE II
SUBJECT INFORMATION

ID	Age	Height	Weight	Injury	Stage
1	26	182cm	80kg	RACI	Post-injury, 1 year
2	23	180cm	75kg	LACL	Post-surgery, 8 months
3	20	178cm	77kg	RMI	Post-injury, over 1 year
4	22	181cm	90kg	LPI	Post-injury, 1 year
5	22	178cm	75kg	LACLM	Post-surgery, 3 months
6	20	183cm	77kg	LACLM	Post-surgery, 8 months

L: Left; **R**:Right; **ACI**: Articular cartilage injury; **ACL**: Anterior cruciate ligament rupture; **MI**: Meniscus injury; **PI**: Patellar injury; **ACLM**: Anterior cruciate ligament rupture with meniscus tear.

The training period occurred over three weeks and involved 2 courses (2 weeks+1 week, Fig. 8).

1) Pretreatment follow-up.
2) First optimal stiffness measurement.
3) First course of treatment.
4) Second optimal stiffness measurement.
5) Second course of treatment.

Peak torque [76] (PT), average torque [77] (AT), and average work [78] (AW) in extension and flexion are critical metrics for evaluating the efficacy of rehabilitation. The torque of the knee was measured according to the derived biomechanical model (see Fig. 6). The mechanical friction moment of the robot was measured at 30 Nmm by swinging the shank rod without explicitly generating motor resistance, *i.e.*, the minimum resistance torque of the robot is 30 Nmm. Gravity compensation was performed by measuring each subject's passive limb torque at 30° of knee flexion. Five submaximal warm-up leg swing repetitions were performed before each subject performed consecutive maximal-effort extension and flexion repetitions. The torque sensor was periodically tared to accommodate temperature drift.

At the beginning of each rehabilitation course (Course 1 and Course 2), the optimal stiffness of the robot was determined using a comprehensive indicator (CI). The CI encompasses peak torque, average torque, and average work in a single movement cycle, and evaluates both the extension and flexion portions of movement. The extension metric is denoted as X_{ext} (PT_{ext}, AT_{ext}, AW_{ext}) and is characterized by its intraclass correlation coefficient (ICC) that estimates the reliability of the corresponding data group. ICC itself is calculated as

$$\text{ICC} = \frac{\text{MSB} - \text{MSW}}{\text{MSB} + (n-1)\text{MSW}} \tag{36}$$

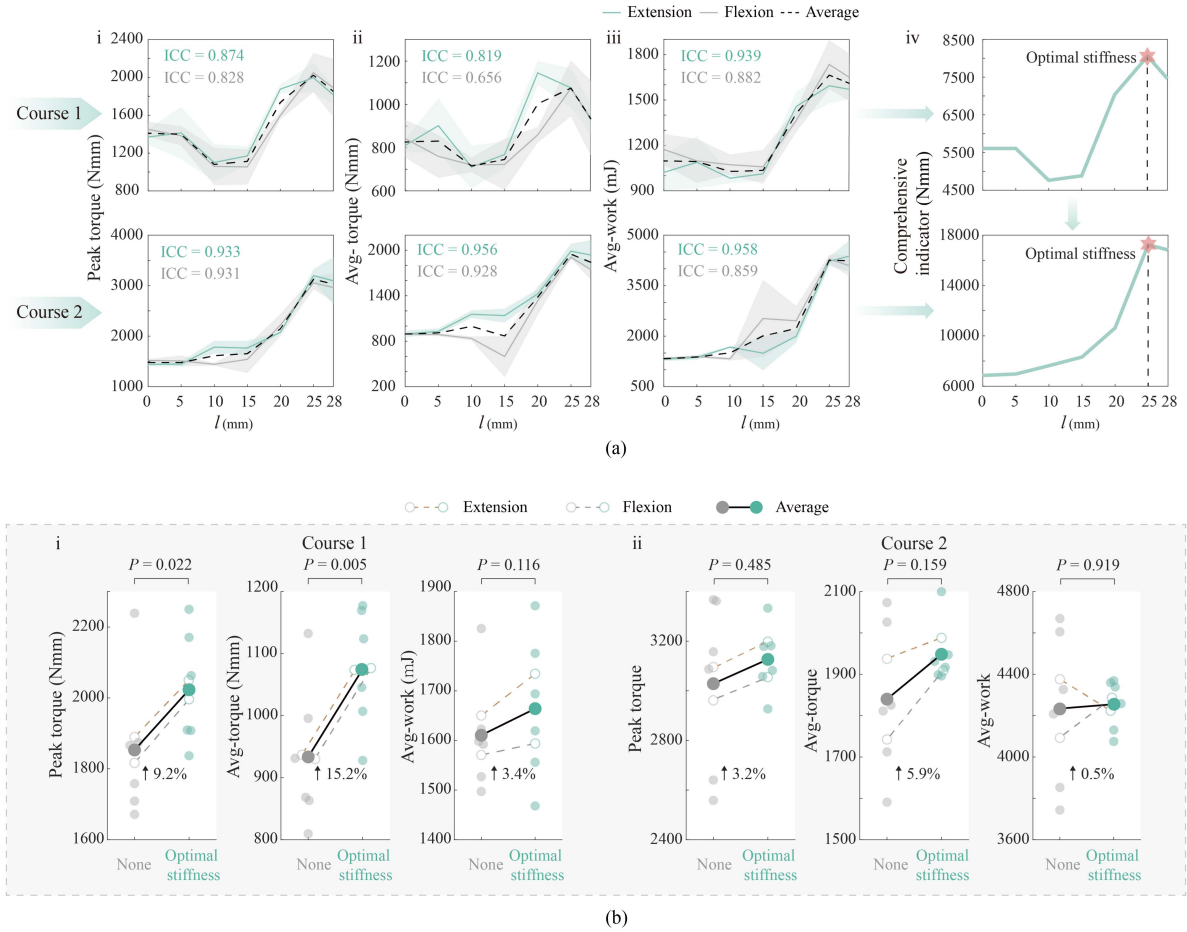

Fig. 9. Optimal stiffness selection as evaluated with Subject 1. (a) Optimal stiffness selection over two trials according to the maximum value of the CI. Optimal stiffness did not change between the two measurements (38.4 Nm/rad, $l = 25$ mm). The ICC was used to measure the reliability of the data group. (b) Improvements in peak torque, average torque, and average work when utilizing optimal stiffness. Gray points represent fixed stiffness at the maximum setting. The green points represent the use of the optimal stiffness. Hollow circles denote group means.

where MSB is the mean square between groups, MSW is the mean square within a group, and n is the number of groups.

Similarly, the flexion metric is denoted as X_{fle} (PT_{fle}, AT_{fle}, AW_{fle}). Overall CI is defined as the sum of X_{ext} and X_{fle} (6 items in total), where each element's corresponding ICC serves as its weight according to (37). This approach provides a comprehensive evaluation of rehabilitation metrics.

$$\text{CI} = \sum \left(\text{ICC}_{X_{\text{ext}}} X_{\text{ext}} + \text{ICC}_{X_{\text{fle}}} X_{\text{fle}}\right). \tag{37}$$

In practice, the subjects were asked to complete five maximal-effort knee extension-flexion repetitions at a velocity of 120°/s to reduce the interference of stiffness measurement on training. To explore the experimental conditions, subject 1 was asked to repeat 10 times (3 sets) first. Meanwhile, the average rehabilitation metrics (peak torque, average torque, and average work) in a single extension-flexion cycle were measured at 7 stiffnesses ($l = 0$, 5, 10, 15, 20, 25, and 28 mm). CIs were calculated by (37). The stiffness (l) corresponding to the maximum CI was selected as the optimal stiffness. For consistency, the optimal stiffness was measured twice during the rehabilitation period (see Fig. 8).

TABLE III
OPTIMAL STIFFNESS

Subjects	Course 1 (Nm/rad)	Course 2 (Nm/rad)
Subject 1	38.4	38.4
Subject 2	137.3	137.3
Subject 3	137.3	137.3
Subject 4	38.4	38.4
Subject 5	137.3	38.4
Subject 6	137.3	137.3

The optimal stiffness selections for Subject 1 over the 2 courses of rehabilitation are shown in Fig. 9(a). After two weeks of training, their optimal stiffness remained unchanged (Subject 1, 38.4 Nm/rad, $l = 25$ mm). The remaining subjects' optimal stiffnesses are listed in Table III. The ICCs of all data groups are greater than 0.6, suggesting the reliability of results [79]. For Subject 1, the detailed comparison of rehabilitation metrics between training at no variable stiffness (maximum stiffness, similar to traditional rigid isokinetic training) and training at optimal stiffness is shown in Fig. 9(b). Utilizing their optimal stiffness in Course 1, Subject 1's average values (mean of

IEEE Transactions on Robotics (T-RO) paper, presented at ICRA 2026, Vienna, Austria. Cite as T-RO paper.

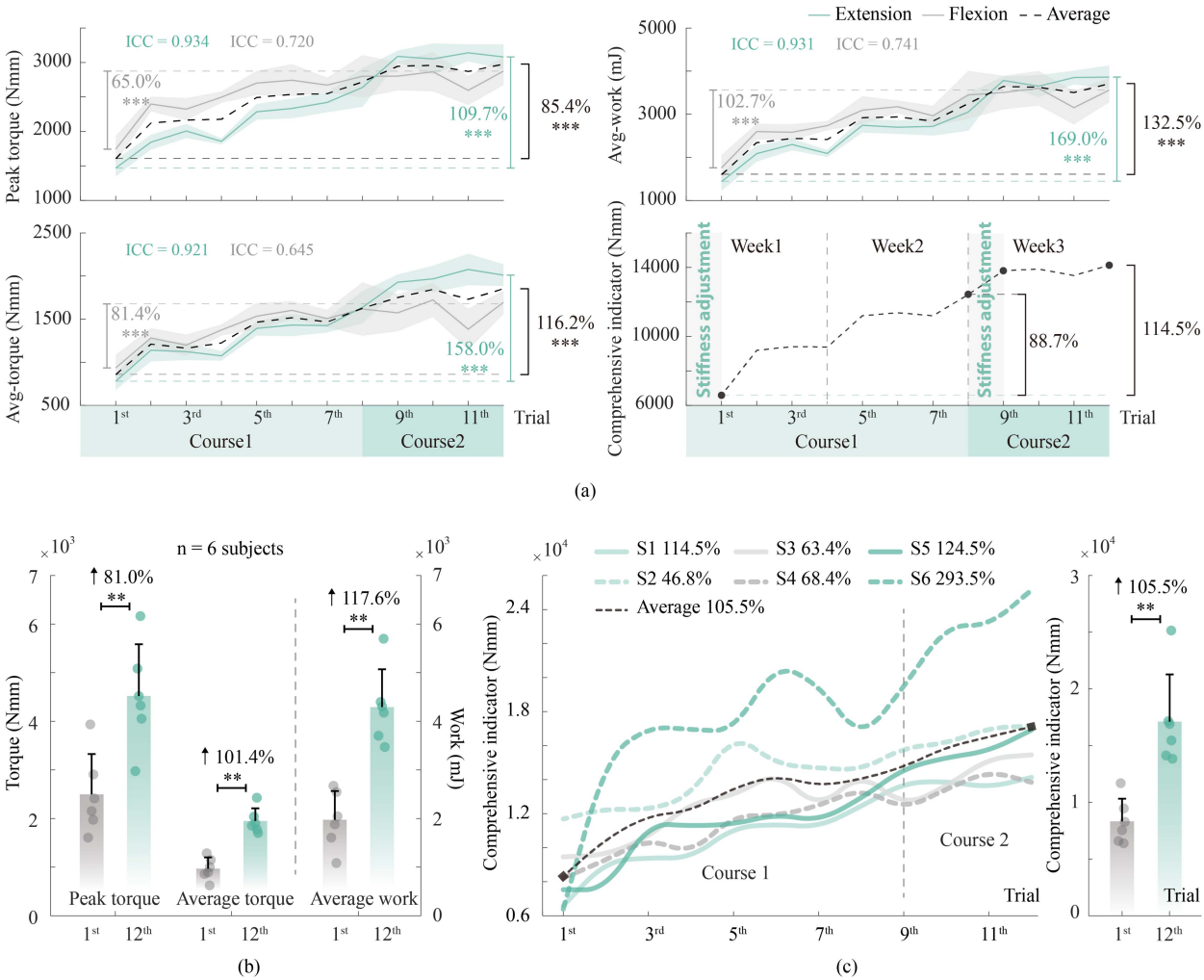

Fig. 10. Clinical improvement after 3-week training period. (a) Metrics of improvement of Subject 1. The subject used the robot to practice by the bedside at 120°/s with settings adjusted to their optimal stiffness (38.4 Nm/rad, $l = 25$ mm). ***P<0.001 (paired-sample T-test). (b) Statistical analyses of all six subjects. Improvements in rehabilitation metrics (mean of extension and flexion) after 12 practice sessions over 3 weeks are shown, including peak torque (PT), average torque (AT), and average work (AW) in one extension-flexion cycle. **P<0.01 (paired-sample T-test). (c) CI from 12 practice sessions. Subject 1 is abbreviated as S1 in this figure, and others follow this convention. Legend numbers represent the growth percentage between 1^{st} trial and 12^{th} trial. **P<0.01 (paired-sample T-test).

extension and flexion data, $n = 3$) of PT_{avg}, AT_{avg}, and AW_{avg} increased by 9.2% (P<0.05), 15.2% (P<0.01) and 3.4%, respectively. Utilizing their optimal stiffness in Course 2, Subject 1's average values of PT_{avg}, AT_{avg}, and AW_{avg}, increased by 3.2%, 5.9% and 0.2%, respectively. The subject performed better after training with the optimal stiffness, suggesting optimal stiffness selection should be done before training for improved outcomes.

C. Clinical Improvement After 3-Week Training Period

A preliminary study involving the six recruited subjects was conducted to assess outcomes of bedside isokinetic training at each subject's optimal stiffness every other day (120°/s, 20 extension-flexion repetitions, at least 8 sets) (see Fig. 8). The bedside training consisted of 12 practice sessions and spanned 3 weeks (23 days). Comprehensive performance tracking for Subject 1 demonstrates improvements over the course of training [see Fig. 10(a)]. Comparing the final data (23rd day, 12th trial) with the initial data (1st day, 1st trial) by using paired-sample T-test, in extension, PT_{ext}, AT_{ext}, and AW_{ext} increased by 109.7%, 158.0%, 169%, respectively (P<0.001). In flexion, PT_{fle}, AT_{fle}, and AW_{fle} increased by 65.0%, 81.4%, 102.7%, respectively (P<0.001). On average, PT_{avg}, AT_{avg}, and AW_{avg} increased by 85.4%, 116.2%, and 132.5%, respectively (P<0.001). For the CI, CI showed a tendency for gradual growth. At the end of the course 1 (15th day, 8th trial) and the end of the course 2 (23rd day, 12th trial), the CI increased by 88.7% and 114.5%, respectively, compared to the beginning of each course.

Rehabilitation metrics for all six individuals are summarized in Fig. 10(b) and (c). As shown in Fig. 10(b), the improvements in the metrics' population mean are all significant. Specifically, peak torque increased by 81.0% ($P = 0.007$), average torque increased by 101.4% ($P = 0.003$), and average work increased

TABLE IV
COST ESTIMATION

Items	Cost($)
Machine work (batch production)	179
3D-printing	73
Sensors	60
BLDC motor	70
Straps	7
Circuits and electronic components	100
Total	489

by 117.6% ($P = 0.005$). For the CI, a significant improvement was measured as an increase of 105.5% over baseline values ($P = 0.008$). Subject 6 demonstrated the highest growth rate of 293.5%, and the lowest growth rate observed was 46.8% [see Fig. 10(c)]. Consequently, the strengths of knee extensors and knee flexors in all participants were significantly improved as a result of the 3-week training period, suggesting that the robot is effective for bedside knee rehabilitation within this timeframe.

IV. DISCUSSION

A. Device Comparison

Despite its efficacy, isokinetic training has remained difficult to implement in bedside knee rehabilitation due to the high cost, bulk, and rigidity of existing devices. These qualities make them unsuitable for bedridden patients or individuals with weak muscles [20], [21], [22], [23], [24]. We addressed these challenges by developing a light-weight (1.3 kg), low-power (0.45 ± 0.01 W), and cost-effective (<$500, Table IV) bedside isokinetic robot that bridges the gap between bed rest and subsequent isokinetic training when ambulatory. Compared to other wearable devices [34], [35], [37], our robot also demonstrates superiority in the aspects of power consumption, volume, weight, and human–robot interaction (see Table I). By incorporating dynamic energy regeneration and variable joint stiffness, the robot is able to accommodate a wider variety of subjects outside of the hospital.

B. Efficacy

Utilizing the bedside isokinetic robot, six individuals with knee impairment showed significant improvements in average peak torque (81.0%), average torque (101.4%), and average work (117.6%) during knee extension-flexion exercises over the course of a 3-week training period. These improvements in muscle tone suggest that bedside isokinetic training may be able to expedite the timeline for bedridden patients to regain ambulation. Moreover, the proposed robot was shown to adapt well to a variety of knee impairments due to the subject-specific versatility afforded by the variable stiffness adjustment mechanism. From our modeling of muscles as a VSA (see Fig. 6), it follows that a subject's muscles may be maximally activated if robot joint stiffness can be made to match their muscle stiffness. Indeed, significant improvements (46.8% –293.5%) to rehabilitation metrics were observed for individuals with different knee injuries, such as cartilage injury, anterior cruciate ligament rupture, meniscus injury, and patellar injury. Finally, with an operating time approaching 200 days when utilizing regeneration [11], [12], the robot can feasibly support the complete rehabilitation training cycle for bedridden patients on a single charge. The reduced complexity afforded by this feature may facilitate the satisfaction of regulatory and safety requirements to enable take-home usage without professional supervision.

C. Limitations

To effectively allocate resources commensurate with the uncertainty of our approach, this study was designed to evaluate the effectiveness of the proposed robot within a limited application scope. Hence, we only investigated six participants aged 20–26 years throughout a 3-week trial in an initial feasibility study. Based upon the positive results presented here, we seek to expand both the duration of testing and the participant pool to more clearly define the scope of the application. Further, although the energy regeneration ratio of our device remains relatively low (14.6%) at slower movement velocities around 60°/s, the battery life is still measurably improved compared to having no ability to regenerate at all. Indeed, the efficacy of isokinetic training does not depend on the efficacy of energy regeneration, and any ability to do so should be considered a secondary benefit for practical implementations. That said, we intend to improve regeneration efficiency through electromechanical redesigns that may include features such as additional gearing or alternative flux linkage ratios. Finally, the biomechanical model in this study is mainly utilized to qualitatively explain the differences in the stiffness of human muscles and does not provide an exact theoretical basis for human–robot interactions. It serves to explain the rationale behind our selected training regimen and provides heuristics for parameter adjustment and experimental design. However, a more rigorous treatment of muscle stiffness in the context of human-robot interactions is important and may be covered in future work.

V. CONCLUSION

In this study, we proposed and tested a bedside isokinetic training robot with a highly integrated VSA (5.0–137.3 Nm/rad) and energy regeneration system. We also derived a biomechanical model of HMIs during isokinetic training to relate muscle contraction, stiffness, and energy regeneration. Through these contributions, our robot possesses the ability to attain the optimal stiffness of the robot joint that maximizes knee muscle activation during active isokinetic training. The efficacy of our proposed training approach was preliminarily validated throughout a 3-week study involving six individuals with knee injuries. As a result of training, subjects gained enhanced muscle strength while demonstrating safe interactions with our robot. For bedridden and postsurgery patients with weak knee muscle strength, our bedside isokinetic training robot provides an efficient and cost-friendly approach that may facilitate the transition to subsequent isokinetic training when ambulatory.

APPENDIX A SUPPLEMENTARY FIGURES AND TABLES

TABLE V
PAIRED *T*-TEST OF 6 SUBJECTS

Paired Differences	Mean	Std. Deviation	Std. Error Mean	95%Ci Lower	95%Ci Upper	t	df	P
PT 1^{st} Trial - 12^{th} Trial	-2022.228	1142.139	466.276	-3220.829	-823.626	-4.337	5	0.007
AT 1^{st} Trial - 12^{th} Trial	-981.116	437.296	178.525	-1440.031	-522.202	-5.496	5	0.003
AW 1^{st} Trial - 12^{th} Trial	-2319.334	1179.514	481.535	-3557.158	-1081.509	-4.817	5	0.005
CI 1^{st} Trial - 12^{th} Trial	-8782.285	5108.753	2085.640	-14143.592	-3420.977	-4.211	5	0.008

Ci: Confidence interval; **df**: Degree of freedom; **P**: Significance;
PT: Peak torque; **AT**: Average torque; **AW**: Average work; **CI**: Comprehensive indicator

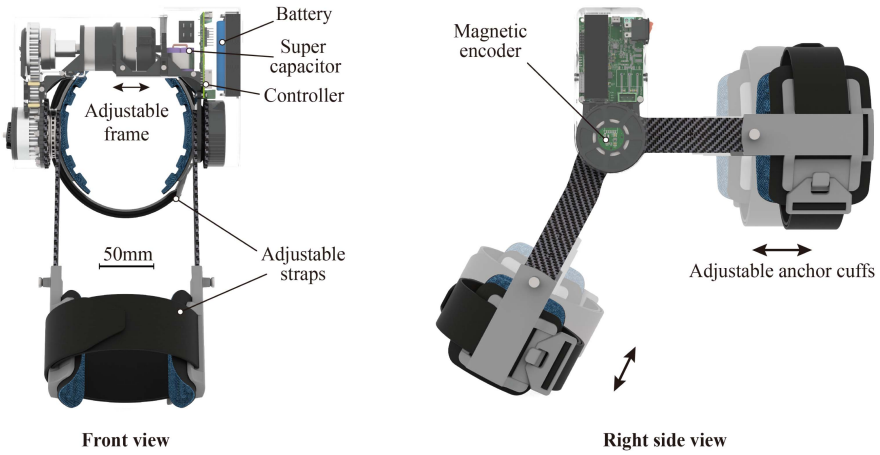

Fig. 11. Front and side view of the proposed robot.

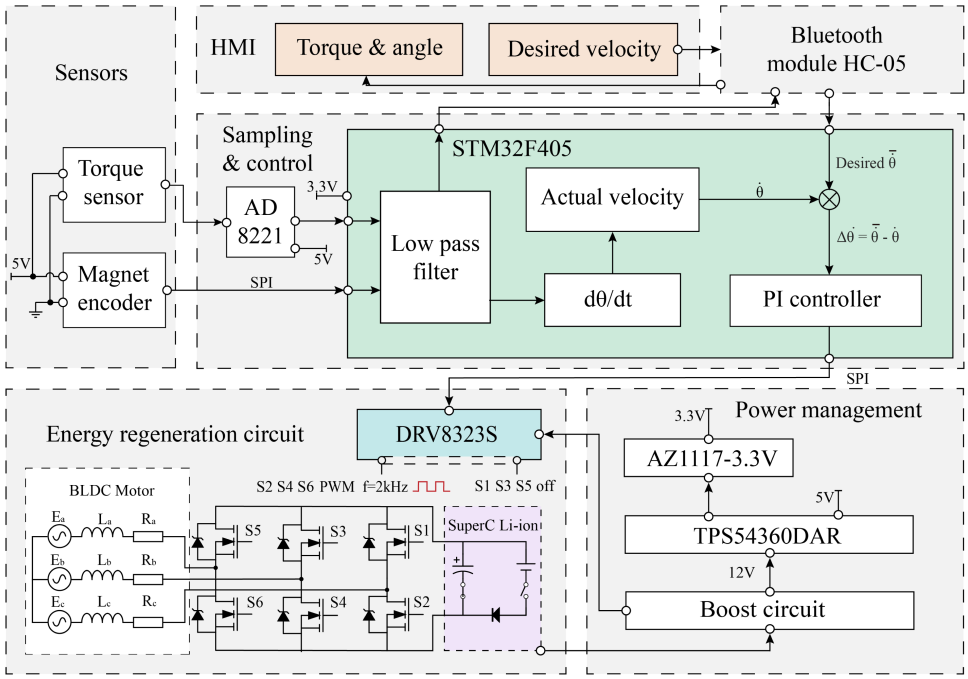

Fig. 12. Detailed design of the circuit.

REFERENCES

[1] D. S. Logerstedt, J. R. Ebert, T. D. MacLeod, B. C. Heiderscheit, T. J. Gabbett, and B. J. Eckenrode, "Effects of and response to mechanical loading on the knee," *Sports Med.*, vol. 52, no. 2, pp. 201–235, 2022.

[2] D. S. Logerstedt et al., "Knee pain and mobility impairments: Meniscal and articular cartilage lesions revision 2018," *J. Orthop. Sport. Phys.*, vol. 48, no. 2, pp. A1–A50, 2018.

[3] B. E. Smith et al., "Incidence and prevalence of patellofemoral pain: A systematic review and meta-analysis," *Plos One*, vol. 13, no. 1, 2018, Art. no. e0190892.

[4] G. J. Van Leeuwen, E. I. T. De Schepper, P. J. E. Bindels, S. M. A. Bierma-Zeinstra, and M. Van Middelkoop, "Patellofemoral pain in general practice: The incidence and management," *Fam. Pract.*, vol. 40, no. 4, pp. 589–595, 2023.

[5] "United nations-summary of results-population division," Report, 2022. [Online]. Available: https://un.org/development/desa/pd/content/World-Population-Prospects-2022

[6] A. Früh et al., "Peripheral nerve stimulation for the treatment of chronic knee pain," *Sci. Rep.*, vol. 13, no. 1, 2023, Art. no. 15543.

[7] C. Djurtoft et al., "Quality of life in adolescents with longstanding non-traumatic knee pain: An analysis of 316 adolescents with patellofemoral pain and osgood-schlatter disease," *Phys. Ther. Sport*, vol. 61, pp. 156–164, 2023.

[8] Y. Yang et al., "Effectiveness of telehealth-based exercise interventions on pain, physical function and quality of life in patients with knee osteoarthritis: A meta-analysis," *J. Clin. Nurs.*, vol. 32, no. 11-12, pp. 2505–2520, 2023.

[9] B. E. Gage, N. M. McIlvain, C. L. Collins, S. K. Fields, and R. D. Comstock, "Epidemiology of 6.6 million knee injuries presenting to United States emergency departments from 1999 through 2008," *Acad. Emerg. Med.*, vol. 19, no. 4, pp. 378–85, 2012.

[10] M. Majewski, H. Susanne, and S. Klaus, "Epidemiology of athletic knee injuries: A 10-year study," *Knee*, vol. 13, no. 3, pp. 184–8, 2006.

[11] B. A. Alkner and P. A. Tesch, "Knee extensor and plantar flexor muscle size and function following 90 days of bed rest with or without resistance exercise," *Eur. J. Appl. Physiol.*, vol. 93, pp. 294–305, 2004.

[12] E. R. Mulder et al., "Strength, size and activation of knee extensors followed during 8 weeks of horizontal bed rest and the influence of a countermeasure," *Eur. J. Appl. Physiol.*, vol. 97, no. 6, pp. 706–715, 2006.

[13] P. Kortebein et al., "Functional impact of 10 days of bed rest in healthy older adults," *J. Gerontol. A-Biol.*, vol. 63, no. 10, pp. 1076–1081, 2008.

[14] R. G. Brower, "Consequences of bed rest," *Crit. Care Med.*, vol. 37, no. 10, pp. S422–S428, 2009.

[15] H. Akima et al., "Inactivity and muscle: Effect of resistance training during bed rest on muscle size in the lower limb," *Acta Physiol. Scand.*, vol. 172, no. 4, pp. 269–278, 2001.

[16] A. Petrucci, D. Guglielmino, J. Pecci, and H. Pareja-Galeano, "The effects of isokinetic training in athletes after knee surgery: A systematic review," *Physician Sports Med.*, vol. 52, no. 4, pp. 309–316, 2024.

[17] D. Verrill, E. Shoup, G. McElveen, K. Witt, and D. Bergey, "Resistive exercise training in cardiac patients: Recommendations," *Sports Med.*, vol. 13, pp. 171–193, 1992.

[18] A. Bahşi, Ö. Altindağ, M. S. Akaltun, A. Aydeniz, E. E. Avci, and A. Gür, "Comparison of the effects of isokinetic, isometric, and isotonic exercises on knee osteoarthritis using ultrasound," *Cureus*, vol. 14, no. 8, 2022, Art. no. e28324.

[19] J. Cabri, "Isokinetic strength aspects in human joints and muscles," *Appl. Ergon.*, vol. 22, no. 5, pp. 299–302, 1991.

[20] U. Gunnarsson, M. Johansson, and K. Strigard, "Assessment of abdominal muscle function using the biodex system-4. validity and reliability in healthy volunteers and patients with giant ventral hernia," *Hernia*, vol. 15, no. 4, pp. 417–21, 2011.

[21] J. Dirnberger, H.-P. Wiesinger, A. Kösters, and E. Müller, "Reproducibility for isometric and isokinetic maximum knee flexion and extension measurements using the isomed 2000-dynamometer," *Isokinet. Exerc. Sci.*, vol. 20, no. 3, pp. 149–153, 2012.

[22] F. M. Impellizzeri, M. Bizzini, E. Rampinini, F. Cereda, and N. A. Maffiuletti, "Reliability of isokinetic strength imbalance ratios measured using the cybex norm dynamometer," *Clin. Physiol. Funct. I.*, vol. 28, no. 2, pp. 113–119, 2008.

[23] N. A. Maffiuletti, M. Bizzini, K. Desbrosses, N. Babault, and U. Munzinger, "Reliability of knee extension and flexion measurements using the Con-Trex isokinetic dynamometer," *Clin. Physiol. Funct. I.*, vol. 27, no. 6, pp. 346–353, 2007.

[24] Y. Kyriakidou, I. Cooper, I. Kraev, S. Lange, and B. T. Elliott, "Preliminary investigations into the effect of exercise-induced muscle damage on systemic extracellular vesicle release in trained younger and older men," *Front. Physiol.*, vol. 12, 2021, Art. no. 723931.

[25] B. A. Phillips, S. K. Lo, and F. L. Mastaglia, "Isokinetic and isometric torque values using a kin-com dynamometer in normal subjects aged 20 to 69 years," *Isokinet. Exerc. Sci.*, vol. 8, no. 3, pp. 147–159, 2000.

[26] Y. Myong et al., "Development and validation of a portable articulated dynamometry system to assess knee extensor muscle strength," *Sci. Rep.*, vol. 13, no. 1, 2023, Art. no. 11887.

[27] K. S. Sung, Y. G. Yi, and H. I. Shin, "Reliability and validity of knee extensor strength measurements using a portable dynamometer anchoring system in a supine position," *BMC Musculoskel. Dis.*, vol. 20, no. 1, 2019, Art. no. 320.

[28] D. J. Oranchuk, C. M. Juneau, S. S. Diewald, J. Neville, and J. B. Cronin, "The validity of a portable strain-gauge apparatus versus a commercial isokinetic dynamometer for evaluating knee extension kinetics," *Int. J. Sports Phys. Ther.*, vol. 19, no. 3, pp. 258–267, 2024.

[29] N. Ciesla, V. Dinglas, E. Fan, M. Kho, J. Kuramoto, and D. Needham, "Manual muscle testing: A method of measuring extremity muscle strength applied to critically ill patients," *JoVE-J. Vis. Exp.*, no. 50, 2011, Art. no. e2632.

[30] J.-Y. Hogrel, O. Benveniste, and D. Bachasson, "Routine monitoring of isometric knee extension strength in patients with muscle impairments using a new portable device: Cross-validation against a standard isokinetic dynamometer," *Physiol. Meas.*, vol. 41, no. 1, 2020, Art. no. 015003.

[31] L. C. Almekinders and J. Oman, "Isokinetic muscle testing: Is it clinically useful?," *J. Amer. Acad. Orthop. Sur.*, vol. 2, no. 4, pp. 221–225, 1994.

[32] T. Kikuchi, K. Oda, Y. Ohyama, S. Isozumi, and J. Furusho, "Development of isokinetic exercise system using high performance MR fluid brake," in *Proc. IEEE Int. Conf. Mechatron.*. IEEE, 2009, pp. 1–6.

[33] A. Keller, J. Hellesnes, and J. I. Brox, "Reliability of the isokinetic trunk extensor test, Biering-Sørensen test, and Åstrand bicycle test: Assessment of intraclass correlation coefficient and critical difference in patients with chronic low back pain and healthy individuals," *Spine*, vol. 26, no. 7, pp. 771–777, 2001.

[34] S. Park et al., "Design and validation of a wearable dynamometry system for knee extension-flexion torque measurement," *Sci. Rep.*, vol. 14, no. 1, 2024, Art. no. 10428.

[35] S. F. Dong, K. Q. Lu, J. Q. Sun, and K. Rudolph, "Rehabilitation device with variable resistance and intelligent control," *Med. Eng. Phys.*, vol. 27, no. 3, pp. 249–255, 2005.

[36] J. Kang, D. Martelli, V. Vashista, I. Martinez-Hernandez, H. Kim, and S. K. Agrawal, "Robot-driven downward pelvic pull to improve crouch gait in children with cerebral palsy," *Sci. Robot.*, vol. 2, no. 8, 2017, Art. no. eaan2634.

[37] J. Nikitczuk, B. Weinberg, P. K. Canavan, and C. Mavroidis, "Active knee rehabilitation orthotic device with variable damping characteristics implemented via an electrorheological fluid," *IEEE ASME Trans. Mechatron.*, vol. 15, no. 6, pp. 952–960, Dec. 2010.

[38] S. Wolf et al., "Variable stiffness actuators: Review on design and components," *IEEE ASME Trans. Mechatron.*, vol. 21, no. 5, pp. 2418–2430, Oct. 2016.

[39] S. Bi, C. Liu, H. Zhao, and Y. Wang, "Design and analysis of a novel variable stiffness actuator based on parallel-assembled-folded serial leaf springs," *Adv. Robot.*, vol. 31, no. 18, pp. 990–1001, 2017.

[40] V. Chalvet and D. J. Braun, "Algorithmic design of low-power variable-stiffness mechanisms," *IEEE Trans. Robot.*, vol. 33, no. 6, pp. 1508–1515, Dec. 2017.

[41] J. Choi, S. Hong, W. Lee, S. Kang, and M. Kim, "A robot joint with variable stiffness using leaf springs," *IEEE Trans. Robot.*, vol. 27, no. 2, pp. 229–238, Apr. 2011.

[42] Y. Wang and L. Fang, "A simple stiffness equation for a variable stiffness joint using a leaf spring," in *Proc. IEEE Int. Conf. Robot. Biomimetics*. IEEE, 2017, pp. 724–729.

[43] P. Bilancia, G. Berselli, and G. Palli, "Virtual and physical prototyping of a beam-based variable stiffness actuator for safe human-machine interaction," *Robot. Com.-Intgr. Manuf.*, vol. 65, 2020, Art. no. 101886.

[44] V. Chalvet and D. J. Braun, "Criterion for the design of low-power variable stiffness mechanisms," *IEEE Trans. Robot.*, vol. 33, no. 4, pp. 1002–1010, Aug. 2017.

[45] L. C. Visser, R. Carloni, and S. Stramigioli, "Energy-efficient variable stiffness actuators," *IEEE Trans. Robot.*, vol. 27, no. 5, pp. 865–875, Oct. 2011.

[46] A. Jafari, N. G. Tsagarakis, and D. G. Caldwell, "A novel intrinsically energy efficient actuator with adjustable stiffness (AwAS)," *IEEE ASME Trans. Mechatron.*, vol. 18, no. 1, pp. 355–365, Feb. 2013.
[47] A. Jafari, N. G. Tsagarakis, I. Sardellitti, and D. G. Caldwell, "A new actuator with adjustable stiffness based on a variable ratio lever mechanism," *IEEE ASME Trans. Mechatron.*, vol. 19, no. 1, pp. 55–63, Feb. 2014.
[48] Z. Y. Yang, S. X. Guo, and Y. Liu, "Preliminary evaluation of a performance-based stiffness control for upper limb elbow joints rehabilitation," in *Proc. IEEE Int. Conf. Mechatron. Automat.*, 2021, pp. 1280–1285.
[49] L. Liu, S. Leonhard, C. Ngo, and B. J. E. Misgeld, "Impedance-controlled variable stiffness actuator for lower limb robot applications," *IEEE Trans. Autom. Sci. Eng.*, vol. 17, no. 2, pp. 991–1004, Apr. 2020.
[50] B. S. Hu, B. H. Mao, S. Lu, and H. L. Yu, "Design and torque control base on neural network PID of a variable stiffness joint for rehabilitation robot," *Front. Neurorobot.*, vol. 16, 2022, Art. no. 1007324.
[51] E. M. Glanzer and P. G. Adamczyk, "Design and validation of a semi-active variable stiffness foot prosthesis," *IEEE Trans. Neural Syst. Rehabil. Eng.*, vol. 26, no. 12, pp. 2351–2359, Dec, 2018.
[52] M. K. Shepherd and E. J. Rouse, "The VSPA foot: A quasi-passive ankle-foot prosthesis with continuously variable stiffness," *IEEE Trans. Neural Syst. Rehabil. Eng.*, vol. 25, no. 12, pp. 2375–2386, Dec. 2017.
[53] C. Everarts, B. Dehez, and R. Ronsse, "Variable stiffness actuator applied to an active ankle prosthesis: Principle, energy-efficiency, and control," in *Proc. IEEE/RSJ Int. Conf. Intell. Robots Syst.*, 2012, pp. 323–328.
[54] R. Riemer, R. W. Nuckols, and G. S. Sawicki, "Extracting electricity with exosuit braking," *Science*, vol. 372, no. 6545, pp. 909–911, 2021.
[55] M. Shepertycky, S. Burton, A. Dickson, Y.-F. Liu, and Q. Li, "Removing energy with an exoskeleton reduces the metabolic cost of walking," *Science*, vol. 372, no. 6545, pp. 957–960, 2021.
[56] J. M. Donelan, Q. Li, V. Naing, J. A. Hoffer, D. Weber, and A. D. Kuo, "Biomechanical energy harvesting: Generating electricity during walking with minimal user effort," *Science*, vol. 319, no. 5864, pp. 807–810, 2008.
[57] L. F. Teixeira-Salmela, S. Nadeau, M.-H. Milot, D. Gravel, and L. F. Requião, "Effects of cadence on energy generation and absorption at lower extremity joints during gait," *Clin. Biomech.*, vol. 23, no. 6, pp. 769–778, 2008.
[58] M. Tran, L. Gabert, S. Hood, and T. Lenzi, "A lightweight robotic leg prosthesis replicating the biomechanics of the knee, ankle, and toe joint," *Sci. Robot.*, vol. 7, no. 72, 2022, Art. no. eabo3996.
[59] A. T. Hamada and M. F. Orhan, "An overview of regenerative braking systems," *J. Energy Storage*, vol. 52, 2022, Art. no. 105033.
[60] X. Nian, F. Peng, and H. Zhang, "Regenerative braking system of electric vehicle driven by brushless DC motor," *IEEE Trans. Ind. Electron.*, vol. 61, no. 10, pp. 5798–5808, Oct. 2014.
[61] Y. Feng, J. Mai, S. K. Agrawal, and Q. Wang, "Energy regeneration from electromagnetic induction by human dynamics for lower extremity robotic prostheses," *IEEE Trans. Robot.*, vol. 36, no. 5, pp. 1442–1451, Oct. 2020.
[62] A. J. Young and D. P. Ferris, "State of the art and future directions for lower limb robotic exoskeletons," *IEEE Trans. Neural Syst. Rehabil. Eng.*, vol. 25, no. 2, pp. 171–182, Feb. 2017.
[63] S. Collins, A. Ruina, R. Tedrake, and M. Wisse, "Efficient bipedal robots based on passive-dynamic walkers," *Science*, vol. 307, no. 5712, pp. 1082–1085, 2005.
[64] F. Gemperle, C. Kasabach, J. Stivoric, M. Bauer, and R. Martin, "Design for wearability," in *Dig. Papers. 2nd Int. Symp. Wearable Comput.*, 1998, pp. 116–122.
[65] S. H. Koo, "Design factors and preferences in wearable soft robots for movement disabilities," *Int. J. Cloth. Sci. Technol.*, vol. 30, no. 4, pp. 477–495, 2018.
[66] V. M. Zatsiorsky and B. I. Prilutsky, *Biomechanics of Skeletal Muscles*. Champaign, IL, USA: Human Kinetics, 2012.
[67] X. Wang, X. Tao, and R. C. So, "A bio-mechanical model for elbow isokinetic and isotonic flexions," *Sci. Rep.*, vol. 7, no. 1, 2017, Art. no. 8919.
[68] I. E. Brown, T. L. Liinamaa, and G. E. Loeb, "Relationships between range of motion, lo, and passive force in five strap-like muscles of the feline hind limb," *J. Morphol.*, vol. 230, no. 1, pp. 69–77, 1996.
[69] A. Remaud, C. Cornu, and A. Guével, "Agonist muscle activity and antagonist muscle co-activity levels during standardized isotonic and isokinetic knee extensions," *J. Electromyogr. Kines.*, vol. 19, no. 3, pp. 449–458, 2009.
[70] T. Yanagawa, K. Shelburne, F. Serpas, and M. Pandy, "Effect of hamstrings muscle action on stability of the acl-deficient knee in isokinetic extension exercise," *Clin. Biomech.*, vol. 17, no. 9-10, pp. 705–712, 2002.
[71] S. Hirokawa, M. Solomonow, Z. Luo, Y. Lu, and R. D'ambrosia, "Muscular co-contraction and control of knee stability," *J. Electromyogr. Kines.*, vol. 1, no. 3, pp. 199–208, 1991.
[72] X. Wang, X. Tao, R. C. So, L. Shu, B. Yang, and Y. Li, "Monitoring elbow isometric contraction by novel wearable fabric sensing device," *Smart Mate. Struct.*, vol. 25, no. 12, 2016, Art. no. 125022.
[73] J.-Y. Guo, Y.-P. Zheng, H.-B. Xie, and X. Chen, "Continuous monitoring of electromyography (EMG), mechanomyography (MMG), sonomyography (SMG) and torque output during ramp and step isometric contractions," *Med. Eng. Phys.*, vol. 32, no. 9, pp. 1032–1042, 2010.
[74] J. Shi, Y.-P. Zheng, Q.-H. Huang, and X. Chen, "Continuous monitoring of sonomyography, electromyography and torque generated by normal upper arm muscles during isometric contraction: Sonomyography assessment for arm muscles," *IEEE Trans. Biomed. Eng.*, vol. 55, no. 3, pp. 1191–1198, Mar. 2008.
[75] M. Laasanen et al., "Biomechanical properties of knee articular cartilage," *Biorheol.*, vol. 40, no. 1, 2, 3, pp. 133–140, 2003.
[76] D. G. Maciel et al., "Peak torque angle, acceleration time and time to peak torque as additional parameters extracted from isokinetic test in professional soccer players: A cross-sectional study," *Sport. Biomech.*, vol. 22, no. 9, pp. 1108–1119, 2023.
[77] T. W. Kaminski and G. C. Dover, "Reliability of inversion and eversion peak-and average-torque measurements from the biodex system 3 dynamometer," *J. Sport Rehabil.*, vol. 10, no. 3, pp. 205–220, 2001.
[78] K. Takey, O. A. Kandil, and S. A. Elazm, "Isokinetic quadriceps peak torque, average power and total work at different angular knee velocities," in *Nat. Conf. Phys. Ther. Cairo*, 2009, pp. 1–14, Conference Proceedings.
[79] G. Perinetti, "Statips Part IV: Selection, interpretation and reporting of the intraclass correlation coefficient," *S. Eur. J. Orthodont. Dent. Res.*, vol. 5, no. 1, pp. 3–5, 2018.

Yanggang Feng received the Ph.D. degree in dynamics and control from the College of Engineering, Peking University, Beijing, China, in 2019.

Subsequently, he joined the University of Tokyo, Tokyo, Japan, as a Postdoctoral Researcher. He currently is an Associate Professor with the School of Mechanical Engineering and Automation, Beihang University, Beijing, China. His research interests include wearable robotics and AI.

Dr. Feng is an Associate Editor of IEEE TRANSACTIONS ON NEURAL SYSTEMS AND REHABILITATION ENGINEERING.

Xingyu Hu received the B.Eng. degree in mechanical engineering from the School of Automation, Beijing University of Post and Telecommunications, Beijing, China, in 2022. He is currently working toward the M.S. degree in robotics engineering with the School of Mechanical Engineering and Automation, Beihang University, Beijing, China.

His research interests include variable stiffness joints, wearable robotics, and rehabilitation robots.

Yuebing Li received the B.Eng. degree in robotics engineering from China University Of Mining And Technology-Beijing, Beijing, China, in 2023. He is currently working toward the M.S. degree in mechanical engineering and automation from Beihang University, Beijing.

His research interests include exoskeletons and wearable robot.

Ke Ma received the B.Eng. degree in mechanical engineering from Beihang University, Beijing, China, in 2023. He is currently working toward the M.S. degree in mechanical engineering and automation from Beihang University.

His research interests include artificial intelligence and robotics.

Jiaxin Ren received the B.Eng. degree in mechanical engineering from Beihang University, Beijing, China, in 2024. She is currently working toward the Ph.D. degree in mechanical engineering and automation from Beihang University.

Her research interests include wearable exoskeletons and rehabilitation robot.

Zhihao Zhou (Member, IEEE) received the Ph.D. degree in dynamics and control from Peking University, Beijing, China, in 2017.

Then, he joined the Beijing Innovation Center for Engineering Science and Advanced Technology in Peking University as a Postdoctoral Researcher. He is currently an Assistant Professor with the Institute for Artificial Intelligence, Peking University, Beijing, China. His research interests include wearable systems and rehabilitation robots.

Fuzhen Yuan received the M.D. degree and the Ph.D. degree in sports medicine from Peking University, Beijing, China, in 2012 and 2019, respectively.

She currently serves as an Attending Physician with the Department of Sports Medicine, Peking University Third Hospital, specializing in foundational research and surgical interventions for knee joint injuries and arthritis. Her academic focus encompasses knee joint replacement, ligament reconstruction, and stem cell therapy.

Yan Huang received B.S. degree in mechanics and the Ph.D. degree in dynamics and control from the College of Engineering, Peking University, Beijing, China, in 2007 and 2012, respectively.

He is currently a Professor with the School of Mechatronical Engineering, Beijing Institute of Technology, Beijing. His current research interests include human movement science and dynamics and motion control of humanoid robots.

Liu Wang received bachelor degree from University of Science and Technology of China in 2014 and Ph.D. degree from University of Texas at Austin in 2019.

He is currently a Professor with the Department of Modern Mechanics, University of Science and Technology of China. His research is focused on soft machines and flexible structure for healthcare applications, including soft robots, soft materials, flexbile devices, human–machine interface, and 3D printing. He has authored or coauthored more than 70 SCI papers such as Science Robotics, Science Advances, Nature Biomedical Engineering, Nature Communications, Advanced Materials, PNAS, etc.

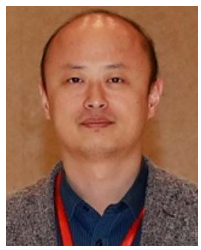

Qining Wang (Senior Member, IEEE) received the Ph.D. degree in dynamics and control from Peking University, Beijing, China, in 2009.

He is currently a Full Professor with the College of Engineering, Peking University. He serves as the Vice Dean with the College of Engineering, Peking University. He has authored or coauthored more than 200 scientific papers in international journals and refereed conference proceedings. His research interests include wearable robotics and humanmachine interfaces.

Wuxiang Zhang (Member, IEEE) received the Master's degree in mechatronics engineering from the Huazhong University of Science and Technology, Wuhan, China, in 2004, and the Ph.D. degree in mechatronics engineering from the Beihang University, Beijing, China, in 2009.

Currently, he is a Professor of mechanisms and machine science with the School of Mechanical Engineering and Automation, Beihang University. His research interests include variable topology mechanisms, exoskeleton robot, space robot and industrial automation.

Xilun Ding received the B.Eng. degree in mechanical engineering from the Zhengzhou Institute of Technology, Zhengzhou, China, in 1991, and the M.Eng. degree in mechanical design and the Ph.D. degree in mechatronics and automation from the Harbin Institute of Technology, Harbin, China, in 1994 and 1997, respectively.

His research interests include the dynamics of compliant mechanical systems and robots, nonholonomic control of space robots, dynamics and control of aerial robots, and biomimetic robots